7-25-2018

Characterizing Late Pleistocene and Holocene Incision and Flooding Post-Glacial Southern New England

Thomas Schenck
University of Connecticut - Storrs, thomas.schenck@uconn.edu

Characterizing Late Pleistocene and Holocene Incision and Flooding in Post-Glacial Southern New England

Thomas Schenck

B.S., Dickinson College, 2008

A Thesis

Submitted in Partial Fulfillment of the

Requirements for the Degree of

Master of Science

At the

University of Connecticut

2018

APPROVAL PAGE

Masters of Science Thesis

Characterizing Late Pleistocene and Holocene Incision and Flooding in Post-Glacial Southern New England

Presented by

Thomas W. R. Schenck, B.S.

Major Advisor_____
William Ouimet

Associate Advisor _____
Robert Thorson

Associate Advisor _____
Michael Hren

Associate Advisor _____
Anjali Fernandes

University of Connecticut

2018

Acknowledgements

I first must thank Dr. Will Ouimet for the guidance and direction for my research. He provided the opportunity, connections, and experience that made this thesis possible. I need to also thank all those on my committee each of whom played a part in this research. Dr. Robert Thorson whose past work in the region provided part of the impetus to study New England kettle ponds looking for floods; Dr. Anjali Fernandes who provided her expertise with sediment suspension; and Dr. Michael Hren for providing help in the field and his expertise and lab space for performing LOI.

I need to thank the Center for Integrative Geosciences at the University of Connecticut for funding and supporting me through the past two years of work. I thank all the faculty and students who provided support while I worked. I need to thank Dr. Lisa Park Boush for her dedication to setting up a coring group at UConn and for her help getting the funding get the basics needed for coring. I also thank the people from the department who came out and helped me in the field, Dawn Beamer, Kevin Langlois, Sam Loeb, and Dana Yakabowskas; without them I wouldn't have been able gather a fourth core.

The cost and field collection requirements needed for this project were many and it wouldn't have been possible without the funding and help of the KECK Geology Consortium and the students involved in taking advantage of the joint research opportunities provided. The work of Sally Donovan, Chad Fagan, Mary Ignatiadis, Jia Kelleher, Caitlin McManimon, and Jacky Tran made my field work possible.

There were many people from different institutions who provided Will and I with critical advice and services for our coring procedure. Drew Hyatt of Eastern Connecticut State shared his expertise on sediment coring, particularly suggesting the use of a farmers jack over a tripod which was a godsend out in the field. I want to thank Pete Dawson, Mike Rhodes, and Brian Yellen from the University of

Massachusetts Amherst for their help in training me in various parts of coring procedure, XRF analysis, and allowing us to temporarily use space in the fridge room at UMASS. I have to thank Brian Yellen in particular for graciously allowing me to stay at his home while performing the XRF scans.

Finally, I must thank the Connecticut Department of Energy and Environmental Protection and Eversource Energy for giving us access to the different field sites across Connecticut.

Table of Contents

List of Figures

List of Tables

List of Appendices

Abstract

Kettle ponds represent localized accommodation space for sediment deposition that can be reliably linked to processes following de-glaciation. For river adjacent kettle ponds the kettle depression traps flood-born material, preserving flood frequency and alterations of the fluvial system. Following glacial retreat New England experienced isostatic rebound as the ice load dropped there were climate oscillations and vegetation changes, all of these factors somehow leading to incision of rivers across southern New England. The evidence of riverine incision into the post-glacial landscape is found across New England and a river adjacent kettle pond preserves the reduction and changes in sedimentation caused by the lowering of river channel beds with respect to a known stable post-glacial elevation of the kettle rim. This study examines the sedimentary archive to explore the evidence for, and timing of, river incision in Southern New England from the Late Pleistocene into the Holocene.

There is an extensive body of work examining ponds and lakes in New England (Brown et al., 2000; Cook et al., 2015; Davis and Ford, 1981; Fallon et al., 2013; Munroe, 2012; Newby et al., 2000; Parris et al., 2010; Patton and Handsman, 1984; Thorson, 1995; Yellen et al, 2014), and though lacustrine sediment consistently preserves flood events, the lake itself is acting as a local base level and so obscures evidence of incision. Examination of isostatic rebound from continental unloading and relative sea level suggests periods of dropping base level for New England Rivers (Koteff et al., 1993; Oakley and Boothroyd, 2012; Stone, 2005) as well as an increasing north/south gradient. The result of the combined uplift and gradient changes would force some incision of rivers into the glacial material making up their channel beds. However, though there is much study and contention concerning the timing and magnitude of rebound, the changes in moisture and the succession of various species, there has been no work done establishing the impact and timing these factors have on river incision.

The study used the sedimentary archive preserved in river adjacent kettles and sediment traps located along the Mount Hope River, Willimantic River, Quinebaug River, and Housatonic Rivers all in Connecticut. Sediment cores were collected for study from each site using a vibracore rig with either 10 ft or 20 ft core tubes. Cores were analyzed and sampled for organic content, radiocarbon aging, grain size, elemental XRF, and Magnetic Susceptibility. The sedimentary analyses of each core were also partnered with paleo-flood recurrence estimation utilizing discharges estimated from modern channel geometry; USGS flood records, and requisite flow velocities to suspend core material. The paleo-flood estimation supported evidence of incision found through LiDAR 1 m DEM investigation of each site.

Analysis in all four cores revealed that between 12,000 to 9,000 yr BP there was a change in sedimentation across all sites. Each site showed higher clastic inputs, coarser grain sizes and lower organic content below the transitional period. The sedimentary change exhibited in both organic content and reduced geochemical markers associated with freshly mobilized material. Though similar transitions from clastic to organic dominated accumulation have been seen in marshland cores from many regions of New England, having the same signature in river adjacent traps with no re-initiation of routine fluvial derived sedimentation points to a period of incision during this transition which left the kettles abandoned.

Introduction

The late Pleistocene to present geologic history of New England is a case study of landscape response to deglaciation, base level adjustments, and changes in vegetation and climate. The retreat of the Laurentide Ice sheet from southern New England between 16,000-20,000 yr BP (Stone, 2005; Thorson, 19095) left an abundance of glacial sediment across New England. Stream terraces are well-documented in the region (Stone et al., 2005; Nicoulin, 2014) and attest to geomorphic adjustment to changing post-glacial conditions along river drainages throughout the region, but few constraints on the age of incision exist. Potential drivers of incision include isostatic rebound from glacier retreat and eustatic sea level changes (Hooke and Ridge, 2016; Koteff et al., 1991; Oakely and Boothroyd, 2012; Stone, 2005), as well as hydrologic events and surface processes (Bradford et al., 2010; Brown et al., 2000).

Following glacial retreat the newly exposed glacial material was available to be reworked by meteoric streams (Davis and Fords, 1981; Stone, 2005). As an erosive environment, there are limited opportunities to preserve the depositional records of incisional events within the southern New England uplands where the erosion has occurred. Kettle ponds, created by buried ice-blocks left by the retreating glacier and now adjacent to river drainages but not directly connected, present reliable conditions to preserve sediment from glacial retreat onward (Benn and Evans, 2010; Jones, 2015). Accessible by streams during flood, the kettle depressions within river valleys provide accommodation space for the accumulation of sediment transported in suspension by the fluvial systems. The frequency at which floods reach and deposit material into a kettle pond is a function of stage-discharge relationships dictated by local climate, precipitation, and storm regimes of the climate (Brown et al., 2000; Knighton, 1998) and of the channel elevation relative to the kettle lip elevation. Deposition records preserved in

lacustrine and marsh environments (Brown et al., 2000; Hubeny et al., 2011; Jones, 2015; Newby et al., 1998; Shuman et al., 2002) may preserve sediment mobilization but not incisional timing as their sediment source remains tied to the base level of the site.

This study examines the record of late Pleistocene and Holocene flooding in New England preserved in river adjacent kettle ponds and sediment traps. The work presented explores the issue of river incision and flooding by investigating four sediment cores using bulk organic content, sedimentological analysis (grain size), and elemental analysis (X-Ray Fluoresence and Magnetic Susceptibility) combined with flood frequency and paleo-flow analysis. The approach used in this study combines the methodological approaches used for paleoflood, fluvial deposit, and lacustrine sedimentation analysis (Brown et al., 2000; Cook et al., 2015; Davis and Ford, 1981; Fallon et al., 2013; Munroe, 2012; Newby et al., 2000; Parris et al., 2010; Patton and Handsman, 1984; Thorson, 1995; Yellen et al, 2014) applying them to previously under-utilized kettle ponds and provides a new method of for the interpretation and classification of sediment preserved in perched sediment traps (active for the last ~17ka) that lie adjacent to modern river courses. Four cores were collected from sites across Connecticut (Figure 1). The core sites were located within the Thames and Housatonic River watersheds; along the Mount Hope, Willimantic, Quinebaug Rivers, and at the confluence of the Housatonic and Ten Mile Rivers. There is no local sediment input at these sites, only floods large enough to overtop the topography surrounding the kettle pond can deposit sediment into the ponds, making them archives of flooding events which were able to reach the kettle at early periods in the river's evolutionary history.

Background

Deglaciation

The retreating Laurentide ice sheet deposited material across the southern New England landscape (Patton, 1988). In this period of ice retreat, ice flow was directed into valleys which were filled with lobed ice, lagging slightly behind the ice clearing from the highlands (Davis and Ford, 1981). Deposition within the valleys by ice lobes created multiple sediment dammed glacial lakes, the largest of which in New England was Glacial Lake Hitchcock in the Connecticut River Valley (Nicoulin, 2014; Patton, 1988; Stone, 2005). As the continent rebounded without the overburden of ice, these glacial lakes were drained as their beds were tilted by uplift progressing from Long Island Sound northward. During early initiation of post-glacial rebound, before the eventual forest take-over of New England, high flow regimes and limited ground cover during early tundra vegetation colonization provided river systems in the wake of the glaciers with high sediment loads; some studies from New England lakes puts the sediment transport from upland to lowland in this early period as up to 30 times to modern rate of transport (Davis, 1993). However, rapid colonization of vegetation stabilized the post-glacial landscape. The changes in vegetation species over time represent a succession of tundra, boreal forest, and temperate forest species showing the transition from cold and dry to modern temperate and wet conditions (Davis and Ford, 1981; Hubeny et al., 2011; Newby et al., 2000; Peteet et al., 2012; Stone, 2005; Thorson, 1995). From periods of low cover and high runoff, filling and breaching glacial lakes, to vacillating climate forcing and vegetation change, the history of New England follows the alteration and adjustment of the landscape in the wake of glaciers.

Kettles

Kettles are depressions created by the melting of buried or partially buried ice blocks which separated from the glacier. Ice calving, differential ablation or topographic variation leads to ice blocks separating from the glacier front (Benn and Evans, 2010). Provided the sediment flux rate from the glacier to the glacier front is high enough the ice block can be buried by material. Glacial meltwater or meteoric water will fill kettles and depending on the permeability of the substrate beneath the kettle the water can be retained, creating a pond. The kettle depressions provide accommodation space for the accumulation of sediment transported by fluvial systems or overland flow: depending on drainage area and ground cover. As kettles form during glacial retreat kettle ponds can reliably preserve material for deglaciation onward by creating a body of still water where flood-born or overland transported material can settle.

Holocene Climate

The transition from a cold, near glacial conditions to modern temperate woodland setting was punctuated by a series of climatic variations that occurred post glaciation. Directly following glacial retreat from southern New England 17,000-20,000 yr BP local climate warmed and vegetation fairly rapidly colonized the newly exposed terrain (Davis and Ford, 1981; Peteet et al., 2012; Stone, 2005; Thorson, 1995) the climate of Southern New England changed from one dominated by albedo to an insolation dominant climate (Shuman et al, 2002). The trend in rising mean average temperature and vegetation colonization post-glaciation has been linked to the changing pollen assemblages found in in New England sediments (Davis and Fords, 1981; Oswald et al., 2009; Shuman and Donnelly, 2002). Immediately following glacial retreat, New England was dry, lacking vegetation. During this early dry period of a few thousand years there was little land cover and conditions provided for significant aeolian mobilization of sediments (Stone, 2005). Records show southern New England tundra becoming

populated by sparse open spruce woodland ~12,500 yr BP with the expansion of mixed temperate forest species beginning ~10,000 yr BP (Davis and Ford, 1981). Once forests were fully established in New England tree cover of various species persisted until clearing by humans following European settlement.

Between 12,900 – 11,600 yr BP was the climate period known as the Younger Dryas (Oswald et al., 2009; Shuman and Donnelly, 2005). This period marked a cooling of the climate across New England, bringing a change in dominant vegetation due to thermal forcing (Davis and Fords, 1981). Following the Younger Dryas event at the beginning of the Holocene pollen records indicate that until roughly 8,000 yr BP the climate in the North Atlantic was warmer than the Younger Dryas (Davis and Fords, 1981; Newby et al., 1998; Shuman et al., 2002). During the same period, current consensus holds that New England was drier than during the Younger Dryas, and up to 4°C warmer than the modern climate (Oswald et al., 2009). Evidence for a dry early Holocene comes from observations of wetland cores from across southern and central New England which record a shift from clastic sediment dominated, lacustrine material to a thick accumulations of peat with lowered clastic percentages (Hubeny et al., 2011; Guerrera et al., 2011; Newby et al., 1998; Oswald et al., 2009; Neurath and Newton, 2008; Shuman and Donnelly, 2005), this change from lacustrine to marsh has been interpreted as a lowering of water levels due to reduced rainfall. The climatic shift back to wetter and slightly cooler conditions 8,000 yr BP coincides with the final collapse of the Laurentide Ice Sheet in Hudson Bay. This collapse completed the progressive change in North America from an ice-sheet and insolation dominated climate to insolation dominant climate which would have altered atmospheric circulation patterns for the north-eastern Atlantic region (Shuman et al., 2002). Levels roughly equivalent to modern (as of 1998) yearly rainfall was reached close to 3,200 yr BP (Newby et al., 1998).

Post-Glacial Isostatic Rebound

The channel slope of a river in equilibrium is controlled by the elevation of the local base level, which is controlled by eustatic sea-level rise and tectonic uplift due to glacial unloading. In southern New England the uplift from isostatic rebound is recorded by the deposits of Glacial Lake Hitchcock and gives an uplift profile of 0.89 m/km toward Hudson Bay (Oakley and Boothroyd, 2012). The increased uplift progressing north from Long Island Sound raised New England with a gradient from the north to south. Studies of isostatic uplift support that on scales <300 km isostatic rebound of New England is non-linear, with a half-life on the order of 1500-2000 years (Oakley and Boothroyd, 2012; Stone, 2005); however, Koteff et al, 1993 argues against delayed uplift and presents a linear rebound directly following glacial retreat. Total values of isostatic rebound are not well-established with a split between rebounds of <35m (Oakley and Boothroyd, 2012) and a rebound of ~75m (Stone, 2005). The current prevailing theory has rebound delayed after ice retreat begging ~16,500 yr BP for Long Island Sound and progressing northward (Oakely and Boothroyd, 2012; Stone, 2005). There is contention over the length of time isostatic rebound persisted, with theories on fast and slow rebound depending on models assuming thick ice or thin ice over New England, though most studies agree that rebound of southern New England had ended between 11,000 and 10,000 yr BP (Oakely and Boothroyd, 2012, Koteff et al., 1993). During the period of glacial melting and tectontic rebound eustatic sea level was also increasing from the melting glaciers; however, relative sea level of rivers draining toward Long Island Sound did not match eustatic sea level. During the initiation of glacial retreat the apparent base level of Connecticut Rivers would have been Glacial Lake Connecticut (present day Long Island Sound) which was completely drained by 15,500 yr BP (Stone, 2005). With the draining of Glacial Lake Connecticut and the continental forbulge ahead of the glacial margin relative sea level dropped from 17,500 to 14,000 years ago, after

which point it began to rise matching eustatic sea level (Oakely and Boothroyd, 2012; Oldale, 1980; Stone, 2005).

River Incision

When base level drops, a river responds by incising, adjust the river profile a new equilibrium (Johnson, 2012). Given some rapid change in base level or resistant piece of channel, the creation of the new steady state river profile can progress upstream from base level as a knickpoints, defined as abrupt changes in channel slope (Johnson, 2012; Nicoulin, 2014). The knickpoints are locations of active incision created by a drop in base level. The establishment of a new equilibrium channel profile adjusted to the new base level propagates upstream as a knickpoint. As rivers establish new channels and abandon old channels, the abandoned channel routinely only partially fills with sediment, leaving a distinct channel shaped depression. New channels are created within the active floodplain (Pye, 1994), so the presence of abandoned channels located outside and in terrain above the modern floodplain indicates some degree of incision. The incision of the fluvial channel into the local floodplain and establishing a new equilibrium channel elevation creates river terraces. River terraces are floodplains, abandoned and incised into when a river base level drops and establishes a new, lower floodplain (Nicoulin, 2014). The level of a terrace can be used as an indicator of paleo-channel levels.

It is important to understand why rivers incise when describing the behavior of southern New England rivers post-glaciation. River incision is controlled by changes in channel slope, discharge (Q), and sediment supply/type (Nicoulin, 2014). Incision occurs from the erosion of channel bed material due to shear stress from passing fluid or from abrasion due to already mobilized sediment. The ability of a flow to entrain and transport material is controlled by shear velocity (u_*), grain diameter (D), particle density (ρ_s) and water density (ρ), and gravity (g) which describe the entrainment potential Θ in shields transport equation (Pye, 1994):

$$\theta = \frac{{u_x}^2}{gD(\rho_s - \rho)}$$

As shear velocity is dependent upon discharge the erosive potential of a river can be approximated as a function of contributing drainage area (*A*), surface gradient (*S*), and some dimensional resistance to erosion (*K*), with non-dimensional constants *m* and *n* (Howard, 1994):

$$Q = KA^m S^n$$

Local climate controls the volume of water supplied to the drainage area and while the channel slope controls flow velocities. The upland rivers response to uplift, environmental, and sea-level change would increase the factors that allow for sediment transport so would be expected to have some degree of incision post-glaciation (Stone, 2005).

The primary sedimentation into an adjacent sediment trap (such as a kettle) relates directly to the relative elevation between channel bed and the kettle rim as the threshold for flood depth. Lowering the level of the channel increases the requisite discharge required to deposit material into a kettle, whose rim elevation remains constant. Incision of the channel bed will reduce the frequency of kettle inundation by floods, which in the sedimentary record could appear to be the same as a drop in flood frequency due to climatic driven drops in precipitation. So the complete geomorphic history preserved in the sedimentary record within river adjacent kettles must be interpreted with the inclusion of any indications for incision.

Flooding

Flooding events of a river are driven by large scale precipitation events or changes in ground cover during precipitation events. The frequency of flooding events of a river is therefore indicative of the moisture levels of the climate in which that river is present (Knighton, 1908). Comparing the recurrence rates of higher and lower stage flood events provides the recurrence interval of a flood,

which thus demonstrates amount of normal annual rainfall compared to the frequency at which higher than average rainfall events impact the watershed.

During flood events, discharge increases and the mean velocity within the primary channel increases. This raises the size and number of grains entrained within the flow. Once entrained a grain is kept suspended in the flow or bounces along the stream bed through saltation (Pye, 1998). Of particular interest are the suspended grains, an idealized spherical grain of diameter *D* and density ρ_s which remain aloft due to a balance between the force of gravity F_g shown by

$$F_g = (\rho_s - \rho)\frac{\pi D^3}{6} g$$

and the force of drag F_D on a sphere of cross section *A* falling at velocity ω_s

$$F_D = C_D \rho A \frac{{\omega_s}^2}{2}$$

Where C_D is the constant coefficient of drag (Dietrich, 1982). The coefficient is often dependent on experimental conditions and requires an accurate calculation of cross-sectional area. Grains will remain in suspension so long as turbulent forces upward, which are directly dependent on net flow velocity, prevent the particle from settling back onto the bed (Dietrich, 1982). The mixing of the suspended load vertically is a function of grain size and flow velocity, the upper portion of a flow will consist of lower concentrations of the larger fraction of suspended material (Pye, 1998).

Suspended material is transported into the overbank zone by flood waters; the size of material transported there is then dependent on the depth of water overflowing the channel banks. Where overbank flow encounters a depression such as a kettle, the flow velocity drop with the increased flow area and material moving as suspended load or bedload over the floodplain will become deposited. When discharge is high enough, some flow enters and leaves the kettle, maintaining enough velocity to keep the finest grains in suspension. The coarser fraction of suspended load settles and is then preserved as an “event deposits” layer of increased coarse fraction relative to the surrounding material.

Study Area

This study utilized material gathered from four location in the highlands of eastern and western Connecticut (Figure 1) adjacent to rivers within the Thames River and Housatonic River watersheds. The underlying geology of the western site consists of bedrock of granites and metamorphic carbonates, schists, and gneiss while the eastern sites consist of bedrock of just granite, schists, and gneiss; with all four sites consists of overlain by glacial sediment. The kettle ponds and deep marsh at these field sites were established during glacial retreat ~20-17 ka (Boone and Eyles, 2001; Glover et al., 2011; Benn and Evans, 2010).

The Mount Hope River (MHR) site (41°48'20" N, 72°9'59" W) is a roughly circular kettle with a 15 m diameter located along the Mount Hope River (Figure 2). The site is located 8 miles into the 10 mile long Mount Hope River watershed, which has a total drainage area of 72 km^2 , part of the greater Thames River watershed. The field site itself is 88 m above sea level. The closest USGS gage site used for local flood records is site 01121000 near Warrenville, CT, which is 2.6 miles directly upstream of the field site. The modern channel bed is composed of primarily coarse gravel, cobbles, and few boulders armoring a bed of gravel and sand. The field site is perennially inundated from the winter until mid-late summer depending on rainfall and currently has no rooted vegetation, hosting only duckweed during periods of inundation (Appendix 5). The kettle rim is 3.5 m above the modern channel but the topography separating the channel and the kettle has a minimum elevation of ~4m above the modern channel bed.

The Willimantic River Rest Stop (WRRS) field site (41°53'25" N, 72°18'2" W, Figure 2) kettle is located near the I-84 rest stop in Willimantic, CT 113 m above sea level. The site is a circular kettle, host to a modern marsh, ~22m in diameter (Figure 2). The field site is located in the middle of the Willimantic River watershed, which has a total drainage of 132.6 km^2 and is part of the greater Thames

River watershed. The USGS gage station used in for flood records of the site is station 01119500 near Coventry CT, a station 9.8 miles downstream of the field site. The field site is located within 200 m of interstate 84, however the lack of any construction tailings, debris, or cleared trails observed at or around the site established that there not been any recent anthropogenic impacts due to road construction. The modern kettle is permanently inundated and is dominated by *Cephalanthus occidentalis* (common name) growth sitting on top of the peat. The lowest point separating the kettle from the modern Willimantic River is a small depression in the surrounding hill that is ~4.5 m above the channel bed (Figure 2).

The kettle pond field site adjacent to the Quinebaug River (SBQB) is located within Sugarbrook Park in Plainfield, CT (41°43'25" N, 71°57'5" W, Figure 3) at 37 m above sea level. The Quinebaug River watershed consists of 2,200 km^2 shared between Massachusetts, Connecticut, and Rhode Island. The USGS gage station recording flooding for this site was station 01127000 at Jewett City, CT, which was 8.7 miles downstream of the field site. The kettle sampled is the largest (minor axis 16 m, major axis 41 m) of three irregularly shaped depressions located within a terrace above the Quinebaug River (Figure 3). At the site are two terraces and a potential third terrace/modern flood plain. Across the river from the site, as well as three, and five miles upstream are sand and gravel quarries gathering material form Glacial Lake Quinebaug deposits. The modern channel at the sampling location has mixed bed of sand to large cobbles. The kettle depressions are shallowly inundated in the spring. To flood the kettles water must reach a height of ~8 m above the modern channel bed.

The Housatonic and Ten Mile field site (HSTM) is located near the New York border in the southwestern corner of Kent, CT at the confluence of the Housatonic and Ten Mile Rivers (Figure 3, 41°40'7" N, 73°30'45" W) 92 m above sea level. The Ten Mile River watershed covers ~520 km^2 while the Housatonic River has a watershed of ~1,422 km^2 across New York, Connecticut, and Massachusetts. The USGS gage station used as a record of floods for the field site is station 01200500 at Gaylordsville,

CT, which was 21.8 miles upstream of the field site. The site is located in a glacial till platform within what is interpreted as an abandoned paleo-channel meander located adjacent to a terrace (Figure 3). The marsh at HSTM is larger than other sites and is an active wetland rather than pond, hosting a wider range of wetland and water tolerant plant species. The water table is located near the surface of the marsh and does actively drain west toward the Housatonic River. The wetland at the site is actively fed by a stream flowing in at the wetland's northern apex (Figure 3). During raised water levels in the wetland water drains through a stone wall down through the paleo-channel, into a small marsh before reaching the Housatonic (Cross section Figure 3). The point where water drains from the marsh is ~10 m above the channel bed where the Ten Mile River joins the Housatonic River. The southern portion of the paleo-channel separating the marsh from the Ten Mile River is ~13 m above the Housatonic/Ten Mile confluence channel bed; however, the slope of the Ten Mile River is such that the same location is only ~10 m above the closest point in the Ten Mile channel (Figure 3). The modern channel bed of the Ten Mile River is primarily gravel to large cobble, while the Housatonic is a gravel/cobble bed river with some gneiss bedrock sections.

Methods

Field Procedure

Three of the four field sites were located using a 1m LiDAR (Light Detection and Ranging) bare earth digital elevation model. The fourth field site was chosen because it was the location of a previous Master's research project in 1996 (Bugden, 1996) which performed a hydrologic study as well collected and dated a core from the site. Sites were chosen based on river proximity, distance from human impacts, site accessibility, and a raised topography separating the kettle from the active floodplain. Following site location, each site was verified to be a deep bottomed depression which before coring by using a 6m soil probe.

Core Collection and Preparation

We retrieved one core per site with a standard vibra-core system using 20 ft and 10 ft, 3 in diameter 1/32 in wall aluminum pipe. Field accessibility and probed depth determined whether a 10 ft or 20 ft pipe was used. The cores of MHR and WRRS were taken to a depth of refusal, taken to be basal gravel rich till based on the history of the area (Bugden, 1996; Stone, 2005). SBQB and HSTM were taken to a maximum penetration depth allowed by the aluminum tubing available and did not encounter impenetrable layer.

Sediment cores were split laterally for description, photography, sampling, and geochemical analysis. Upon splitting, both halves of the cores were cleaned using a steel paint spatula or knife. After cleaning, both cores were allowed to dry for 10 hours. After initial drying to make layering visible one half of the core was photographed then transferred from the aluminum pipe to a PVC pipe, cut into 1.5 m segments and each sealed in plastic wrap for transportation to the University of Massachusetts,

Amherst. The other half of the core was let dry further if layering was still only partially visible, then used for stratigraphic description (Appendix 6-9) and destructive analysis.

Core Description and Geochemistry

The core halves that were taken to the University of Massachusetts, Amherst were brought the university XRF Laboratory where each core was scanned with an ITRAX X-ray fluorescence (XRF) core scanner (Cook and Yellen, 2015). The scanner used a molybdenum X-ray source (30 kV and 55mA) and measured XRF at 1 mm increments with exposure time of 10 seconds. 33 elemental signatures were recorded per XRF scan. The specific mineral abundances in cores determine the usefulness of specific elements, with many having no applicable correlation within the studied cores. Based on the findings previous XRF studies (Berntsson et al., 2015; Brown et al., 2000; Cook and Yellen, 2015) combined with comparison to LOI, it was determined K, Fe, Ti, Si, Rb, and Zr correspond to clastic material. For this study, Potassium (K) were used as a metric for mineral content based the previous work of Yellen and the highest correlation with LOI measurements. Magnetic susceptibility (MS) was measured at 5 mm increments with a residence time of 5 seconds.

Core descriptions were performed upon drying a section of core enough that compositional variation could be easily seen. Core descriptions were based on visual identification of compositionally distinct units within each core. Description noted visible organics, layering, and grains to be used in conjunction with other methods to establish a site geomorphic history.

Core Sample Analysis

2 cm thick samples were taken at either 10 cm increments or two samples per described unit, whichever sampling method provided a denser sampling subset. Extra sediment samples were extracted from visibly identifiable coarse layers, defined by a greater portion of visible sand and larger grains, along with samples above and below such layers.

Samples were dried at 100°C for 10 hours and mass water lost measured. Each sample was physically disaggregated before heating for loss on ignition measurement. Dried and disaggregated samples were heated to 545° for 4.5 hours for and mass lost was attributed to lost organic carbon. After LOI baking, samples were sieved to fractions greater and less than 63 μm; % finer than 63 μm is equivalent to % clay. The fraction greater than 63 μm was analyzed with a CAMSIZER measuring individual grain area and number of grains counted. Grain sizes from the CAMSIZER were reported in the diameter of a spherical grain with area equal to the measured grain. Sorted by percent composition by weight (assuming grain density of 2.7 g/cm^3) analysis for samples used the grain size of which 50 and 90 percent by weight were finer, D50 and D90. The size classes for D50 and D90 were reported from raw calculation of all grains by the CAMSIZER software. Grain sizes that were able to be measured had a maximum minor axis of 10000 μm.

Material submitted for ^{14}C dating were selected from primary plant matter. Three samples were taken from MHR, four from HSTM, and two from SBQB (Appendix 6). Samples were washed and floated in distilled water to remove as much clastic material as possible. Each sample was then dried and sent to the NOSAMS Facility at Woods Hole Oceanographic Institute, Massachusetts, which performed sample cleaning, preparation, and age calculations for the accelerator mass spectrometer dates (Appendix 6). Preparation involved heated acid bath leaching up to 20 times to remove inorganic carbon and organic acids. The sample material is then combusted producing CO_2 which is reacted with a Fe catalyst to form graphite, the graphite is then ionized in the mass spectrometer and the ^{14}C fraction measured.

Paleo-Flood Estimation

A flood is a period of increased discharge in a fluvial system, with discharge defined by the equation $Q=WDV$, where Q is discharge and V is mean flow velocity. A flood of a given discharge will fill

a channel valley to a specific depth (and so width) dependent upon the average flow velocity. Considering that any flood which could deposit material into the river adjacent kettle must have a depth greater than the topography between the kettle and river, some flood estimation is possible. This study is based on the assumption that sediment within the kettles is deposited by floods, so an estimation of potential floods within the studied regions informs interpretation of the sediments. The estimation of paleo-floods uses the known depth and an estimation for the width and velocity of flows capable of depositing material into the kettles to reconstruct paleo-discharge and compare it to modern discharges.

Estimating the width for paleo-floods using the modern channel was made from measurements from LiDAR 1m DEM of the site with the projected extent of a flood of the requisite depth (Appendix 13). A wide and narrow width measurement was taken from each projection to give a high and low bound for flood estimation. To project the flooded depth for a given area the local DEM was converted to elevation above nearest channel bed. The adjustment to the DEM was accomplished by recalculating the elevations with respect to local channel bed at given points, and adjusting using the measured channel slope from the unaltered DEM. A second set of widths were taken from the request depths required to flood the lower terrace at the Quinebaug site.

Velocity estimations for paleo-floods were performed using two methods, solving Manning's equation for the modern geometry and suspension velocities calculated from grain size analysis. The Manning's equation for depth average velocity, *v*, is:

$$v = \frac{1}{n} R^{2/3} S^{1/2}$$

Where *S* is the average channel gradient, *R* is the hydraulic radius and *n* is Manning's roughness coefficient which is based on impediment of flow by bodies in the channel. This study used the

approximation that *R* is effectively equal to depth, *D*, for channels where *D* << *width*. The equation then becomes

$$v = \frac{1}{n} D^{2/3} S^{1/2}$$

Depth was taken as the elevation above the modern channel bed of the kettle plus 0.5 m (to estimate a flood which completely fills the kettle and distributes sediment evenly within it) while slope was measured from the modern channel using LiDAR 1m DEM. The depth averaged velocity was calculated twice using two values for Manning's roughness *n* values for a high and low boundary for velocity. The roughness values used were *n*=0.065 and *n*=0.11 based estimates of floodplain and channel roughness by Chow, 1959 and considering the width of the channels compared to widths of the floodplains in the measured cross sections (Figure 2,3; Table 2).

The depth average velocity calculated from grain size analysis used the D50 of grain size samples from event deposits. To find the settling velocity ω_s for some idealized particle of diameter D_n a method put forth by Dietrich, 1982 was used. Given the particular relationship

$$\log W_* = -3.76715 + 1.192944(\log D_*) - 0.09815(\log D_*)^2 - 0.00575(\log D_*)^3 + 0.00056(\log D_*)^4$$

for dimensionless settling velocity W_* in a fluid of kinematic viscosity *v* and a dimensionless particle size D_* shown by

$$W_* = \frac{\rho {\omega_s}^3}{(\rho_s - \rho) g v}$$

$$D_* = \frac{(\rho_s - \rho) g {D_n}^3}{\rho v^2}$$

So using the D50 as D_n ω_s could be solved for. The calculation of depth averaged velocity uses the assumption that given a shear velocity (u_*) three times the settling velocity of a particle, the net turbulent velocity would be enough such that all those grains would be suspended load (Smith, 1997).

The depth averaged velocity ($\bar{u}$) was calculated using an estimated drag coefficient of 0.002 and the relationship from Dietrich, 1982 that

$$\bar{u} = \sqrt{\frac{u_*}{C_D}}$$

The D90 was not used for this analysis because of the potential for entrainment of large particles from the floodplain as bedload or saltation due to flow irregularities created by vegetation on the flood banks.

The flow velocity from each estimation method was then used to calculate discharge using the measured widths and projected depths from the previous measurements. The calculated discharge was used to solve for recurrence interval based on the frequency-discharge relationship established from the peak discharge records from of nearest USGS stream gauge with the longest records (Dunne and Leopold, 1978). The relationship of the modern channel discharges and recurrence interval was calculated using Excel trend line tools on the peak discharge plot (Appendix 15). Given the presence of clear terraces at SBQB a recurrence of floods originating from a channel with a theoretical 1 m depth below the terrace was calculated using the Manning method (Table 2, Table 3).

Results

Radiometric dates were gathered from three of the four cores studied (MHR, HSTM, and SBQB) while the fourth core (WRRS) utilized dates gathered during a previous study of a correlated core taken 1.5 m away in the same kettle by Thorson and Bugden, 1995. All radiometric samples and ages are summarized in Table 1. From the MHR core three samples of woody material was taken from samples at 125 cm, 200 cm, and 266 cm depth. The calibrated ages, increasing with depth, were 14181±234 yr BP, 14619±337 yr BP, 15286±256 yr BP. Material that was dated from the previous work at WRRS used wood, peat, and ragweed pollens as dated material. The date's reported correlate to compacted depths in WRRS at 36 cm (3540±50 yr BP), 65 cm (7100±70 yr BP), 90 cm (10440±70 yr BP), and 198 cm (11470±150 yr BP). Two samples of material were collected from SBQB for radiocarbon dates, both woody fibers. The SBQB Calibrated core ages were 3645±34 yr BP at 53 cm and 13478 ±112 yr BP at 224 cm. The HSTM core had four pieces of woody material dated taken from depths of 44 cm, 156 cm, 363 cm, and 482 cm. The material from HSTM had calibrated ages with increasing depth of 3642±37 yr BP, 7902±35 yr BP, 10441±44 yr BP, and 12,855±87 cal. yr BP (Table 1).

Core Analysis

MHR: Mount Hope River

The Mount Hope River core had a recovered length of 320 cm from a penetration depth of 336 cm. The core was divided into seven stratigraphic units based on visual characteristics (Appendix 6); between the seven units there were seven identified layers of sand and gravel (Figure 4). The core is predominantly clastic with LOI below 20% mass lost deeper than 35cm and climbing to a maximum of 40% mass lost above 35 cm. The LOI assessment of organic content matched the visual identification of peats.

The lowest section of core (323-244 cm) designated unit I, showed clearly defined layering between varying mineral and compressed peat layers. Average organic content was below 10%, with the highest organic content being 16% at 268 cm representing a layer with visible compressed plant material. The unit contained three event deposits of fine white/grey sands at 305, 279, and 265 cm. The coarse deposits were differentiated primarily by a decrease in clay content from neighboring samples of up to 80%. The sand layer at 265 cm, nearly 2 cm thick, had visible fining of material at the upper and lower contacts, with the upper contact having a more dispersed fining. Only the lowest event deposit showed a significant increase in the coarser fraction beyond the surrounding material, the other layers were enriched in grain sizes found in other samples in the unit. Ignoring event deposits, the unit showed clay content increasing with depth with the upper samples having 80±10% clay. Sorting in the lower unit varied, with non-event deposit D50 showing little correlation to specific clay content but with a variance in the entire unit less than 500 µm. Average K counts increased slightly upward, from 1000 to 1500 counts/10s. MS decreased in the area of a K increase, corresponding to a clay and sand layer at 279 cm. K values are for sand layers are expected to not directly correlate due to the influence of X-ray scattering by quartz grains and the potential for the detector to not be positioned directly over a coarser layer.

Unit II in the MHR core (244-214 cm) was compositionally similar to the unit below in both organic content and measured K, though it lacked any event deposits. Organic content was below 10% while percent clay was between 80% and 90%. This unit was less clearly divided into layers and had less energetic input during this time, demonstrated by the variance of D50 and D90 (Figure 4).

Unit III (214-110 cm) could be divided into two sub-units based. Sorting decreased from the prior unit between 214 cm and 176 cm with clay content being averaging 45%. The sample at 185 cm was not visibly coarser, but had a D90 of 5259 µm, 4500 µm larger than samples above or below, while the D50 was 232 µm varying by less than measurement error from nearby samples. The presence of

well mixed material matches a drop decrease of average K counts. MS decreases initially and increases to previous values, suggesting some mineralogic variation. The upper half of unit III contained a 2 cm woody piece centered at 163 cm, this corresponds to a negative MS and drop anomalous drop to near 0 K counts. Samples from higher in the unit did not include the larger pieces of woody debris present form 170 cm to 110 cm thus the organic content only increased by 5%. However, the pieces of woody material are reflected by drops in the measured MS and K counts. From 110 cm to 97 cm there is only homogenous clay, corresponding to a rise in K counts and MS, this region was designated unit IV. From 97 cm to 43 cm was divided into two units (Appendix 6). Unit V has a distinct transition from a region stained orange by oxidized iron to an underlying dark and organic rich layer; above the transition organic content is 3% and MS is ~10, below the transition organic content increases to 16% and MS drops to ~2.

Above unit V in unit VI are four event deposits located at 85 cm, 61 cm, 57 cm, and 44 cm., identified by a yellow coloration, visible sand, and a clay fraction that was 25% less adjacent samples. There was a single highly rounded cobble (minor axis 4 cm) at 84 cm along with a very fine sand layer, D50 524 μm. For MS and K scans the cobble had to be removed leaving an air cavity which produced an anomalous drop in measurements. The three uppermost event deposits were poorly sorted mixes of orange tinted sand and fine gravel, with MS spikes indicating increased iron content. Organic content increases between each layer of the upper most layers from 2% organic at 67 cm to 16.9% at 49 cm. Above the shallowest event deposit K counts decrease with increasing organic content, dropping from an average K counts of 800 to average 100 counts at 30 cm. Above 30 cm is also the beginning of visibly low compaction peats.

WRRS: Willimantic River Rest Stop

The Willimantic River core had a recovered length of 204cm from a penetration depth of 250 cm. The core was divided into 9 visible variations in composition (Appendix 7). Organic content, K, and

MS shows that the core is split into two main sedimentary sequences between 11470 yr BP and 10440 yr BP. The two sedimentary sequences consist of a clastic dominated lower core with organic mass comprising less than 36% of samples and a peat dominated upper core with organic mass comprising more than 78% of samples (Figure 5).

The lower core rises in organic content from 17% at 200 cm to 36% at 141 cm. The percent clays in each sample increases with organic content, from 38% clay at 200 cm to 85% clay at 141 cm. D90 varies but has an overall decrease from the bottom of the core to 141 cm, with grain sizes decreasing from a maximum of 3671 μm to 412 μm. The grain size of the D50 varies between 200 μm and 300 μm in the lower core. MS varies by 1 SI with a slight decrease in average between 150 cm and 141 cm. K counts follow MS values holding average ~800 counts, up to 145 cm where it decreases to ~600 counts before dropping to a baseline of ~50 counts.

Above 137 cm the core is composed of peat with sampled material at 136 cm having percent organic 78% the lowest value for the upper region of the core. Throughout the upper core sample material available for grain size analysis was low as most samples were over >85% clay, with multiple samples having too little material available for grain size analysis. This made the D50 and D90 measurements have a wider sample density. Within the organic dominant upper core were three layers of peat where clay content dropped below 75% and fine sands were present, while the organic content remained the same. These layers were centered at 71 cm, 49 cm and 20 cm. Only the layer at 71 cm was registered with an increase in MS and none corresponded to a rise in K values (as would be expected for sediments well mixed in peat). The K values showed seven peaks above a ~80 count baseline in the organic dominant region, six in unit III and one in unit VI. The peaks were located in regions of lower organic content, between 70% and 80% in unit III, and at 93 cm where organic content drops by 5% respective to adjacent samples (Figure 5).

SBQB: Quinebaug River at Sugar Brook Park

The site located next to the Quinebaug River had a recovered core length of 245 cm, from a penetration depth of 278.5 cm. The core was divided into nine stratigraphic units (Appendix 8). Between the nine units there were five distinct event deposit layers. The centers of the event deposits are at 129 cm, 96 cm, 75 cm, 55 cm, and 20 cm, differing from the other examined cores is the thickness of two of the event deposits described in units III and VI, to be described later (Figure 6).

Unit I of SBQB from 245 cm to 190 cm is a collection of well mixed silt and sand with a few small gravels, similar to unit I of WRRS. The sand and gravels of the lowest unit are composed almost exclusively of white muscovite mica. Sand content and vertical heterogeneity decrease while silt/clay composition remains relatively similar in unit II (190 cm to 136 cm), with visible sands reducing to almost none near the top of the unit. Unit III (136 cm - 126 cm) along with unit VI (100 cm - 88 cm) are event deposits of iron oxide tinged sands and silts. Both units III and VI have a D50 that varies by less than 100 µm from non-sand bearing event deposits. The D90 in unit III is 534 µm, over 200 µm greater than adjacent layers. The D90 of unit VI is substantially coarser than unit III at 978 µm while also containing gravel pieces greater than 1 cm. Between the similar event deposits of unit III and VI is a region dominated by homogenous silts divided into unit IV (126 cm -120 cm) and unit V (120 cm - 100 cm). Unit IV is a layer of dark brow silt mixed with white sand enriched layer, with clay content ~28% and 9% organic carbon. Above unit IV in unit V the predominant silt darkens marginally with a reduction in sand content and increase in organic content: clay content rises to 40-50% and organic carbon increases to 19-28%. Unit VII (88 cm - 73 cm) contains silt and frequent assemblages of white micaceous sands, with a 2 cm event deposit at its upper margin that has depleted fines, a clay fraction 5.8%, and mixing of fine and coarse sand, D50 555µm and D90 2946 µm. Unit VIII (73 cm - 10 cm) contains the highest organic content of the core, up to 88%, and contains two white micaceous event deposits which are cleaned of fine material and organics, less than 10%. One event deposit was at 55 cm which was too thin to sample

and one at 20 cm which contained fine sand to small gravel, D50 of 441 µm, and D90 of 3241 µm. The top 10 cm of the core, unit IX, is a relatively homogeneous layer containing silt and uncompressed grass and root material. There is a distinct contact with unit VIII below which separated upon drying (Figure 6). In unit IX the organic and clay content increased by ~25% over the adjacent sample in unit VIII.

HSTM: Housatonic and Ten Mile

The HSTM core had a recovered length of 515 cm from a penetration depth of 554 cm, having 49 cm of compaction occurring. The core was described with six compositional units in total (Figure 7, Appendix 9). Much like WRRS, there was a transition from clastic material below 350 cm to organic peat above 350 cm, dividing the core into two distinct sedimentary bodies the timing of which occurred closely after 10441 yr BP. Organic content increased upward from 24% carbon at the bottom of the core to a maximum LOI >80% in unit IV, then decreasing back to values between 60% and 70% (Figure 7).

The clastic part of the core, referred to as the lower core, was composed of fine material with some visible laminations and fresh water invertebrate shells, indicative a lacustrine setting. Laminations were generally thicker than 3 mm and disappeared in unit II where there were abundant gastropod and mollusk shells (Appendix 9). Invertebrate shells coincided with the few large pieces of organic material in the lower core, woody material one of which appeared to be a branch. Gastropods and mollusks are no longer present above ~396 cm, indicating a change in lake condition which removed these species. The fine sediments within HSTM were expected to be all much finer than 63 µm, combined with the presence of calcite shells (which would not be removed by LOI) samples from HSTM were not processed for grain size measurement.

XRF analysis of HSTM supported our visual classification of the core, with higher K returns in units I and III vs. unit II (Figure 7). Unit VI showed an increasing mineral signal from 100 cm and higher. The transition between visible clastic materials to only peat visible above unit III greatly resembled the

same style of transition in WRRS (Figure 5 and Figure 7). The timing of the transition is also similar; some point post 10,000 yr BP. Unlike in MHR and WRRS, magnetic susceptibility of the sediments in HSTM showed no correlation with LOI (Figure 7) and does not correlate with any other measured sediment data. It is likely that the minerals within the HSTM core are Fe depleted and so provide very little magnetic signal.

Paleo-Flood Estimation

The modern flood recurrence rating curve calculated for each USGS gage station is shown in Appendix 15. The equation to shown in Appendix 15 was used to calculate the recurrence interval of discharges provided by Manning and D50 settling velocity analysis. The sites for each site had varying distances to the USGS stream gage used for calculation (see Introduction: Study Area). For the given projections of the modern river system predicted recurrence intervals vary by over 3 orders of magnitude based on the measured widths and roughness.

Given the narrowest width and highest roughness in the Mount Hope River the potential recurrence interval to flood 4 m depth was a 248 yr flood. Every other estimation placed the recurrence at minimum of ~14,000 yr flood, while a flood flowing through an opening 135 m across had estimated recurrence intervals greater than 1 million year recurrence intervals (Table 3). The Quinebaug River geometry had predicted recurrence intervals of the required discharge to flood a depth of 8.35 m with a minimum recurrence interval of 750,000 years for the smallest channel geometry. Estimating the discharge to flood the kettle at SBQB from the level of the second terrace at the site (Figure 3) has recurrence interval between 10 yr and 24 myr but has an average recurrence interval to flood the site of 8673 yr (Table 3) for floodplain estimate roughness (n=0.11). The Housatonic and Ten Mile Rivers have predicted flood recurrence intervals over 10^{16} yr in order to flood the modern HSTM site to a depth of 0.5 m. The predicted flood recurrence intervals for the Willimantic River were reasonable, to flood a

depth of 4.7 m given a roughness of 0.11 and width of 98.4 m was a recurrence interval of 366 yr, and 22170 yr for a roughness of 0.065. The widest estimation with the highest roughness provided a recurrence interval of 2608 yr with the highest estimated required recurrence to flood the site as ~615,000 yr (Table 3).

Discussion

There is some correlation between high organic percentage and high percent finer than 63 μm. This is to be expected as the lower energy flows associated with fine deposition also favor uninterrupted growth of peats (Bugden, 1996). Trending among all cores as well is a K signal that is inversely proportional to organic content. This has two reasons; one being that reduced clastic input accompanies more stable conditions in which peat can grow. The second, and most significant reason, is the limitation of the XRF test, with only signals being received from the very surface of the material peat with well mixed sediment will be biased by plant matter obscuring mineral grains from the incident X-rays.

Flood Recurrence Interpretations

The results of the flood estimation show ranges of values 10^{15} to 10^{3} (Table 3) the variability highlights the dependence of predictions on the given channel dimensions and the logarithmic equation used to solve for recurrence interval for a given discharge. There is little agreement in the recurrence interval estimations from the Dietrich settling velocity predictions as well. Climate conditions and channel geometry have changed since late Pleistocene (Oswald et al., 2009). This limits the amount of usefulness projecting a flood recurrence rating curve onto floods 12,000 years ago and measuring discharges based on modern channels. Given the high variance, a purely quantitative interpretation would be flawed, but qualitative interpretations based on the minimum values and the side of the maximum values from both velocity calculation methods does provide some insight.

Based on the high predicted recurrence intervals for MHR, WRRS, SBQB, and HSTM from both Manning and Dietrich methods there is strong evidence supporting the position that the current channel morphology and climate at these sites is not responsible for the clastic material found at these sits. The

youngest dates recovered from each core thus give some time constraint for the establishment of current flood conditions.

The only potential way floods could reach the sites is if the channel bed was closer to the elevation of the kettle or southern New England was significantly wetter than today. The body of research concerned with the region does not support a New England that was wetter to the extent necessary to flood rivers like the Housatonic by 10.5 m (Newby et al., 1998; Oswald et al., 2009; Shuman and Donnelly, 2005) however evidence does support that rivers at the studies locations have incised into the post-glacial material to reach their current elevations (Figure 2 and 3).

By applying the paleo-flood estimation from Manning's equation for a channel 1 m below the terrace 4 m below the SBQB site the recurrence interval of floods is potentially within the time frame preserved within the core (Table 1, Table 2). The site would be expected to be shallowly inundated on the scale of potentially centuries and much more infrequent deep flood inundation by the Quinebaug River when it was active ~4 meter below the kettle lip. This type of scenario matches the upper core of SBQB as discussed later.

There can be an argument made to look at the smaller widths measured for floods in Appendix 13 given the potential for a restriction in channel width causing flow to back up and increase inundation height upstream. However, for these restrictions the channel sides are very steep and according to Chow, 1959, the deeper the flow the lower the effective roughness experienced by that flow becomes. As the steep sided channel causes the central body of the flow to increase in depth at a high rate in proportion to increased width, the effective roughness would decrease. So the reduction in roughness is difficult to estimate but it would still mean that the deeper a flow became, the higher the flow speed could become as it encountered less resistance and thus the required discharge necessary to inundate the sites.

Core Interpretations

Analysis across all the cores showed clear changes in sedimentation across all cores occurring within a time frame of 12,000 to 8,000 yr BP. The strength of the analysis was also shown in the comparison of XRF geochemistry, MS, LOI, and grain size analysis shows the correlations between the different measurements that indicate changes in core composition. However, before further discussing the analysis results first the limitations of the analysis must be discussed to properly inform interpretation. MS influenced by the minerals within the core, if mineral matter is reduced in iron by enough, the difference of magnetic response of the mineral and organic matter will not be particularly different (evidence in HSTM, Figure 7). For The limitation of XRF analysis methods is the fluorescence only measures emission of minerals on the surface of the core. Sediment well mixed into organic matter, particularly fibric peat, is only registered if the mineral matter is present at the surface where the core was laterally split. If plant matter makes up the scanned surface of the core, such as the wood debris in MHR at 163 cm, the XRF registers reduced or no K. So, instead of being analogous to mineral matter found through LOI, the XRF measurement does not perfectly correspond to LOI in fibric peats because of the shielding of mineral matter by organic material.

Three cores—MHR, WRRS, and HSTM—show an abrupt change in LOI and K counts, changing from clastic sediment dominated to organic sediment dominated input (Figure 4, 5, 7). In MHR this transition occurs at a depth of 41 cm and shows a change in LOI from ~10% to ~40% and a drop of 800 K counts at the same location (Figure 4). The percent fines in MHR also stabilizes at ~73% at the organic transition showing very low energy sediment input from a less variable source either local drainage. The variance of the D50 in the upper section, ~170 µm, increases in overall size showing that depositions is by the uppermost water of higher energy flows. HSTM has a similar transition in both LOI and K mineral content, shifting from organic content of 55% to 85% and a drop in average K counts going from ~150

counts to ~60 counts. The K reduction and organic increase in WRRS shows the same trend, and though SBQB shows no organic transition there are other mineralogic transitions. All three of these cores have the change in sediment and composition between 9,000 and 12,000 yr BP. Figure 8 shows the how the potential timing of the depositional change corresponds to similarly timed changes in pollen assemblages and during post-glacial rebound and relative sea level change.

The dates from the MHR core place the sedimentation into the kettle solidly in the late Pleistocene. The averaged sedimentation rate from the Pleistocene conditions lower core was much higher than the Holocene conditions preserved in the upper core, to a surprising degree. The lower core has 141 cm of compressed material accumulated between 14181±234 cal. yr BP and 15286±256 cal. yr BP, compared to 125 cm of material accumulated between since 14181 yr BP and the present. This shows that sedimentation rates at the high/low K transition dropped by an order of magnitude. MS analysis matches the K and LOI observations, supporting the interpretation that total sediment input was reduced. Observing the paleo-channel abutting the site (Figure 2) and considering the gravel material high in the core, it has been interpreted that before the high/low sediment transition the Mount Hope River occupied the visible paleo-channel and at the transition likely altered course and incised to its modern position.

In the HSTM core, above the abrupt clastic/organic transition at 308 cm growth of plants producing fibric peat overtakes sediment input into the site. However, an increase in K counts in Unit VI in the core shows a slight increase in mineral content coinciding with a drop in average organic content to 60% (Figure 7). This should not be considered a re-activation of sediment input from the Housatonic and Ten Mile River but because of how it increases sediment evidence toward the top of the core this suggests the activation of a small stream which feeds into the wetland from the north (Figure 3, Appendix 5). The spikes of K in the upper 100 cm of HSTM should be the result of mineral matter derived from the stream feeding into the marsh from the north. The timing of the mineral input lies

roughly at end of a dry period in New England between 11,500 yr BP and 10,500 yr BP (Oswald et al., 2009). An increase in moisture would lead to the formation of the stream flowing into the marsh and so supply mineral matter to the whole of the marsh during rain, albeit a small quantity.

Analyzing the WRRS core's organic/sediment transitions, the greater than 90% fines content of what little clastic material was available in most of the peat, combined with greater than 80% LOI, shows beyond a few intermittent events the kettle was completely isolated from the nearby river. The increase in D50 in unit VIII and the K peaks after the sediment transition in unit III shows that after transitioning to a sediment starved, peat growing pond intermittent flood waters transporting of at least fine clastic material reached the site up until and potentially after 3500 yr BP. These periodic, isolated increases in mineral content mesh well with the paleo-flood estimations that suggest the potential for a flood to reach the site, albeit very rarely, with a channel geometry close to what it is at present. These layers were most likely formed by floods reaching the kettle as the Willimantic River incised below the elevation of 11,000 yr BP (Figure 8). The lack of organic percentage change with these apparent flood incursions can be attributed to the mixing of sediments by bioturbation and the retarding of flood waters by vegetation. As an active marsh based on the peat assemblage, the center where the core was taken would be shielded by higher energy flood water by the abundant vegetation at the site. This would limit only the upper and easily suspended material reaching the kettle center. The evidence of bioturbation and no change in organic content also shows that the events did not contain enough material to interrupt plant growth.

For SBQB The low organic content of the bottom units of the core are expected for a deep water kettle in an active floodplain; depositing sediment frequently and limiting peat growth. Though the well mixed sand of unit I in SBQB may represent the underlying glacial lake Quinebaug sediment (Stone, 2005), something that cannot be confirmed without deeper sampling. Above the well mixed low organic sands the organic content varies from less than 20% to over 40% depending on the layer. This layering

of high and low organics is suggestive of a shallow kettle with infrequent event deposition, allowing for increased building up of organic material. The change in mineral content and sorting of the distinct event deposits within SBQB shows an abrupt shift in sediment source.

Units III and VI in SBQB likely potentially represent event deposits from flood remobilization of the well sorted material from higher in the sequence of glacial lakes located along the Quinebaug River. The thickness of the two units also implies a large volume of material captured from the water column, something that would be expected for a flood which deeply inundated the kettle; such as when the kettle terrace was the active floodplain (Figure 3). All units above VI were cleaner white material and less well sorted. This change in sediment source available to the Quinebaug River can be attributed to deposition by higher energy flows which were eroding material from freshly exposed material deeper in in glacial lake Quinebaug deposits. The paleo-flood estimation provides evidence for a period of deposition in the core when the Quinebaug River was at the second terrace found at the site (Figure 3). Semi-frequent floods reaching the site, combined with a few high energy flows expected when the river was eroding into the underlying glacial lake Quinebaug while transitioning to a new terrace then occupying the middle terrace, match what is seen in unit VII and VIII in SBQB. The transitional period, during which floods still frequently reach the site but bring new material due to river incision into the old floodplain matches unit VII. The similar white micaecous material surrounded by higher organic and silt content suggests a stable, infrequently lightly flooded and rarely deeply flooded kettle in unit VIII (Figure 6, Appendix 8). The clean, poorly sorted event deposits in the unit are consistent with high energy floods, and their infrequency is partially supported by paleo-flood estimations. The complete transition from one active floodplain to a stable lower plain occurred sometime between 13,000 and 4,000 yr BP, incision initiating during the same period of supposed incision at the other sites (Figure 8).

Comparing all cores other than SBQB, there is a time when each kettle began accumulating increased organic matter. If this transition is partially climatic, it should be expected to see some similar

area in SBQB. In the top of unit V, where organic content begins to rise abruptly below 100 cm this could be evidence of this period. Taking this interpretation, the event deposits of unit VI and previously addressed unit VII, both with gravel content preserved evidence of powerful flooding. The flooding could be the impetus for incision which drives the mineralogic change from unit VI to VII, and potentially incision at other sites. Without more dates a direct correlation is difficult to draw, but the potential for short period of high flows within the channels would initiate incision.

Evidence of Incision

Considering the evidence from cores and paleo-flood analysis incision is expected at each site. Supporting the interpretation of incision as the reasoning behind the previously discussed findings are geomorphic indicators of incision present at each field site (Figure 2 and 3). The marsh at site HSTM where the core was gathered is interpreted to be a potential oxbow lake or even a kettle, overprinted by the paleo-Housatonic and Ten Mile Rivers. Outside the modern active marsh, the depth to basal glacial till is less than 1m and south of the site are scattered emplaced boulders. The distribution of rocks near the marsh suggest either an active channel of cobbles and boulders similar to the modern Housatonic and Ten Mile, or are lag stones left behind by a channel winnowing finer material from a poorly sorted till bed. The location of the site and supposed paleo-channel suggests that the terrace emplaced 15 m above the site was the active floodplain of the river when it was emplaced over the current site.

The Mount Hope River DEM shows a clear paleo channel (Figure 2) though it has partially been modified by construction of a trail. 1.16 m beneath the surface within this paleo-channel is a layer of sand and gravel, likely the paleo-channel bed. At the SBQB site there are two terraces (Figure 3) which clearly show two distinct previous floodplain elevations which the Quinebaug River once occupied. The WRRS field site has a remnant of a river terrace as well (Figure 2). The ubiquity of incision features,

combined with the sedimentary change seen in each core draws attention to what could generate the incision seen at each field site.

Drivers of Incision

Given the evidence in all cores for incision and the physical incision markers at each field site this study considered the potential motivators of the incision. The timing of the sedimentation change in all four cores is somewhere between 12,000 and 9,000 yr BP (Figure 8) depending on location, placing it close to the beginning of the Holocene, at the end of the Younger Dryas cold period (Newby et al, 2000), and close to the end of post-glacial uplift (Stone, 2005). Looking at the changes occurring in New England during this time frame provides some insight into potential drivers of incision and changes in site flooding frequency. As addressed earlier the rebound of the North American plate graded north to south by ~0.89 m/km (Oakley and Boothroyd, 2012). This differential uplift would serve to increase the gradient of rivers flowing north to south, of which all studied sites are. The increased gradient, though small, would provide increased energy for incision.

Vegetation changes can lead to downward incision through bank armoring, forcing channelization of a river directing the expenditure of erosive potential onto the channel bed. Before widespread colonization of southern New England by tree species pre 13,000-11,000 yr BP sediment loads were higher (Figure 8). Solifluction and frost heaving will cause greater sediment destabilization on grassy slopes than on forested slopes. Both processes lead to increased denudation and sediment transport into valley bottoms. In a vegetation study, Davis noted that in watersheds in Southern New England erosion of glacial material 11,750 yr BP was “30 times the modern rate” of nearby forested watersheds (Davis, 1993; Likens et al., 1977). Higher sediment input into valley bottoms would load rivers with material, effectively monopolizing the river’s transport potential over incision. Tree species spread north following the retreat of glaciers and the warming of climate of the region. Of the first

species to colonize New England spruce was the first, arriving in the studied areas some time ~12,000 yr BP. In their work studying watershed changes caused by forest colonization Davis and Ford 1981 noted that "exports of particulate inorganics from [mirror lake] catchment declined dramatically at the time of spruce appearance in the local flora between 12 kya and 11 kya". Without hillslope erosion to resupply material to channel beds and banks stabilized by trees, New England would experience a period of incision.

Another regional change that would be expected to generate incision is the post-glacial isostatic rebound of the region. Post-glacial uplift would raise elevation of headwaters with respect to the ocean while the draining of glacial lake Connecticut would cause a drop the base level, both motivating an increase in channel slope and so erosive potential. The essential condition for both uplift and lake drainage is the change in apparent base level. Additionally, the timing of continental rebound is problematic, with apparent base level of the studied rivers dropping before the sedimentation change at 15,500 yr BP when glacial lake Connecticut drained. The changes in relative sea level during this time-frame do not completely match eustatic sea level which was continuously rising as the ice caps melted. From a period between 18,000 yr BP ending approximately 14,000 yr BP the relative sea level in Long Island Sound dropped due to the progression of a glacial induced continental forbulge passing through the region.

The response to dropping glacial lake levels and rising elevation with respect to sea level could generate a more continuous rate of incision along the entire river channel, leading to gradational changes we don't see in our cores. However, along the length of a river there can be multiple relative base levels created by the sediment dams on pro-glacial lakes and bedrock knickpoints which would create a local base level which is independent of relative sea level. Any breach in the sediment dam in pro-glacial lakes would create region where flow abruptly increased, generating a knickpoint. The rate of migration of the knickpoint upstream could explain the timing of incision supported by the cores. The

passage of the knickpoint past the site would create a new channel geometry and flooding extents in a short period of time. The terraces at HSTM and SBQB (Figure 3) support a more periodic lowering of the equilibrium channel rather than continuous adjustment, potentially due from the passage of knickpoints.

As discussed earlier, similar coring studies performed across southern New England have identified a shift from lacustrine sediment to marsh peat ~10,000 yr BP (Hubeny et al., 2011; Guerrera et al., 2011; Newby et al., 1998; Oswald et al., 2009; Neurath and Newton, 2008; Shuman and Donnelly, 2005) and identified a climatic change reducing water levels as the motivator. The studies marking the sedimentary changes come from isolated drainage basins with no riverine sediment sources. Due to the similarity of the clastic/sediment transition visible in cores from this study, we can assume that whatever climatic change caused the shift there is some connection to the shift in the studied kettles. If the climate did dry and water levels lowered across New England ~11,000 yr BP, river discharge would be reduced, stopping the floods the previously would inundate the studied sites, potentially causing the change in sedimentation we see. Even if the change we see is only driven by dropping water level in the kettle and a vegetation change, there must have been some incision to prevent the adjacent rivers from reaching the sites again after the return to wetter (more modern) conditions ~8,000 yr BP (Oswald et al., 2009; Newby et al., 1998).

Conclusion

The timing of incision of New England Rivers into their glacial till filled valleys is a subject that has not been rigorously studied by the scientific community. Whether the incision occurred as a continuous process or was dominated by shorter periods of intense erosion is still up for debate. However, the sediment cores recovered suggest some period of incision between 12,000 – 9,000 yr BP (Figure 8). There is a comparable transition in isolated marsh cores occurring at a similar time frame across New England, so it must be concluded that the change in the studied kettles was climate driven in the same way that the change in isolated marshes was. However, the similarity with isolated marsh cores does not entirely rule out the evidence for incision in the cores.

What the cores could potentially preserve is somewhat continuous incision throughout the Late Pleistocene and Holocene. Floods routinely overtopped the topography surrounding the study sites, depositing sediment as the rivers adjacent to them slowly incised into the post-glacial landscape. When the climate of southern New England dried ~11,000 yr BP, reduced river discharges ceased bringing floods to reach the kettle sites. During the dry period lasting until ~8,000 yr BP, the studied rivers continued incising into the post-glacial till underlying their valleys so that when the dry period ended, the rivers were lower with periodic floods only capable of very shallow inundation of the sites by the largest floods. Floods from this time on would bring the smallest fraction of suspended material in the water column to be deposited into the kettle site. This interpretation of continuous incision is supported by the timing of the sedimentary shift, which occurred toward the end of isostatic rebound and during a period of relative sea-level rise (Figure 8). The timing of dropping base levels predicted by Oakley and Stone (Figure 8) should have initiated incision of the river profile during that time but relative sea level began rising again during the observed sediment transition. What is likely one of the most important factors in initiating and supporting channel incision is the increase of the north-south

gradient in New England throughout the period of rebound, reaching its greatest once rebound ended. This gradient increase could have provided the necessary flow acceleration, or combined with other factors, to cause incision.

This study showed that river adjacent kettle ponds are effective sediment sinks which can preserve specific instances of flood born sediment deposition. In order to study the environmental changes that occurred across southern New England kettle ponds can be used as sources of sedimentary changes. With the goal of categorizing the incisional response to climate shift of the rivers in New England uplands river adjacent kettle ponds are ideal sites that preserve sedimentary changes brought about by incision and changing flow conditions.

Works Cited

Ambers, R.K.R., and Wemple, B.C., 2008, Reservoir sedimentation dynamics: Interplay and implications of human and geologic processes: Northeastern Geology and Environmental Sciences, v. 30, no. 1, p. 49-60.

Balco, G., Belknap, D.F., and Kelley, J.T., 1998, Glacioisostasy and Lake-Level Change at Moosehead Lake, Maine: Quaternary Research, v. 49, no. 2, p. 157-170.

Benn, D.I., and Evans, D.J.A., 2010, Glaciers and Glaciation 2nd edition: Hodder Education, London, UK, 707 p.

Berglund, B.E., and Ralska-Jasiewiczowa, M., 1986, Pollen analysis and pollen diagrams: Handbook of Holocene Palaeoecology and Palaeohydrology, p. 455-484.

Berntsson, A., Jansson, K.N., Kylander, M.E., De Vleeschouwer, F., and Bertrand, S., 2015, Late Holocene high precipitation events recorded in lake sediments and catchment geomorphology, Lake Vuoksjávrátje, NW Sweden: Boreas, v. 44, no. 4, p. 676-692.

Besonen, M.R., Abbott, M.B., Francus, P., Bradley, R.S., and Ridge, J.C., 2002, High resolution hurricane activity record for southern New England from 1,200 year long varved coastal sedimentary record: Abstracts with Programs - Geological Society of America, v. 34, no. 1, p. 30.

Bierman, P.R., Lini, A., Zehfuss, P., Church, A., Davis, P.T., Southon, J., and Baldwin, L., 1997, Postglacial ponds and alluvial fans; recorders of Holocene landscape history: GSA Today, v. 7, no. 10, p. 1-8.

Boldt, K.V., Lane, P., Woodruff, J.D., and Donnelly, J.P., 2010, Calibrating a sedimentary record of overwash from southeastern New England using modeled historic hurricane surges: Marine Geology, v. 275, no. 1-4, p. 127-139.

Bosley, A.C., Bierman, P.R., Noren, A., and Galster, J., 2001, Identification of paleoclimatic cycles during the Holocene using grain size analysis of sediments cored from Lake Morey in Fairlee, VT: Abstracts with Programs - Geological Society of America, v. 33, no. 1, p. 85.

Brown, S.L., Bierman, P., Lini, A., and Southon, J., 2000, 10 000 yr record of extreme hydrologic events: Geology, v. 28, no. 4, p. 335-338.

Brown, S.L., Bierman, P.R., Mehrtens, C.J., and Lini, A., 1998, Terrigenous layers in lake cores document fluctuations in New England's Holocene climate: Abstracts with Programs - Geological Society of America, v. 30, no. 7, p. 114.

Brown, S., Bierman, P., Lini, A., Davis, P.T., and Southon, J., 2002, Reconstructing lake and drainage basin history using terrestrial sediment layers; analysis of cores from a post-glacial lake in New England, USA: Journal of Paleolimnology, v. 28, no. 2, p. 219-236.

Bugden, W.H., and Thorson, R.M., 1994, Groundwater interaction with a kettle-hole wetland in Connecticut; hydrologic and geochemical evidence: United States (USA), National Ground Water Association.

Cameron, D., 2007, Flow, frequency, and uncertainty estimation for an extreme historical flood event in the Highlands of Scotland, UK: Hydrological Processes, v. 21, no. 11, p. 1460-1470.

Chow, V.T., 1959, Open-channel hydraulics: New York, McGraw-Hill, 680 p

Cook, T.L., Yellen, B.C., Woodruff, J.D., and Miller, D., 2015, Contrasting human versus climatic impacts on erosion: Geophysical Research Letters, v. 42, no. 16, p. 6680-6687.

Davis, M. B., 1983. In Wright H. E.,Jr. (Ed.), Holocene vegetational history of the eastern united states Univ. Minn., Minneapolis, MN

Davis, M. B., and Ford, M. S., 1981, Sediment focusing in Mirror Lake, New Hampshire. Limnology and Oceanography, 27, 137-150.

Dietrich, W.E., 1982, Settling velocity of natural particles: Water Resources Research, v. 18, no. 6, p. 1615-1626.

Donnelly, J.P., Bryant, S.S., Butler, J., et al., 2001, 700 yr sedimentary record of intense hurricane landfalls in southern New England: Geological Society of America Bulletin, v. 113, no. 6, p. 714-727.

Fallon, A.R., Yellen, B.C., Kratz, L.N., and Woodruff, J., 2013, How unique was Tropical Storm Irene? A comparison of deposits from historical floods on the lower Connecticut River: Abstracts with Programs - Geological Society of America, v. 45, no. 1, p. 117.

Farrell, J.C., and Rodbell, D.T., 2012, The sedimentary record of Mohawk River floods preserved in Collins Pond, Scotia, NY confirmed by Hurricane Irene: Abstracts with Programs - Geological Society of America, v. 44, no. 2, p. 85.

Francis, D.R., and Foster, D.R., 2001, Response of small New England ponds to historic land use: The Holocene, v. 11, no. 3, p. 301-312.

Glover, K.C., Lowell, T.V., Wiles, G.C., Pair, D., Applegate, P., and Hajdas, I., 2011, Deglaciation, basin formation and post-glacial climate change from a regional network of sediment core sites in Ohio and eastern Indiana: Quaternary Research, v. 76, no. 3, p. 401-410.

Green, M.J., 2004, Reconstruction of Holocene climate change using image analysis of laminated sediments [Ph.D.]: University of London, University College London (United Kingdom).

Henderson-Sellers, A., Webster, P., McGuffie, K., et al., 1998, Tropical Cyclones and Global Climate Change: A Post-IPCC Assessment: Bulletin of the American Meteorological Society, v. 79, no. 1, p. 19-38.

Hooke, R.L., and Ridge, J.C., 2016, Glacial lake deltas in New England record continuous, not delayed, postglacial rebound: Quaternary Research, v. 85, no. 3, p. 399-408.

Hubeny, J.B., Hammond, B., Morissette, C., Palermo, J.A., Cantwell, M., and King, J.W., 2013, Regional patterns of lacustrine organic matter deposition in eastern New England from the late Pleistocene to present: Abstracts with Programs - Geological Society of America, v. 45, no. 1, p. 123-124.

Hubeny, J.B., McCarthy, F.M.G., Lewis, J., Cantwell, M., Morissette, C., Crispo, M.L., and Zanatta, R., 2011, Holocene stratigraphy and climate history of Sluice Pond, MA: Abstracts with Programs - Geological Society of America, v. 43, no. 1, p. 77.

Jones, A.F., Macklin, M.G., and Benito, G., 2015, Meta-analysis of Holocene fluvial sedimentary archives: A methodological primer: Catena, v. 130, p. 3-12.

Kasprak, A., Magilligan, F.J., Nislow, K.H., Renshaw, C.E., Snyder, N.P., and Dade, W.B., 2013, Differentiating the relative importance of land cover change and geomorphic processes on fine sediment sequestration in a logged watershed: Geomorphology, v. 185, p. 67-77.

Knighton, D., 1998, Fluvial Forms and Processes A New Perspective: Hodder Education, London, UK.

Kochel, R.C., 1988, Extending stream records with slackwater paleoflood hydrology; examples from West Texas: New York, NY, United States (USA), John Wiley & Sons, New York, NY.

Likens, G.E., Bormann, F.H., Pierce, R.S., Eaton, J.S., and Johnson, N.M., 1977, Biogeochemisty of a Forested Ecosystem, Springer-Verlag, New York, N.Y.

Magilligan, F.J., 1992, Thresholds and the spatial variability of flood power during extreme floods: Geomorphology, v. 5, no. 3-5, p. 373-390.

Menking, K.M., Peteet, D.M., and Anderson, R.Y., 2012, Late-glacial and Holocene vegetation and climate variability, including major droughts, in the Sky Lakes region of southeastern New York State: Palaeogeography, Palaeoclimatology, Palaeoecology, v. 353–355, p. 45-59.

Munroe, J.S., 2012, Lacustrine records of post-glacial environmental change from the Nulhegan Basin, Vermont, USA: JQS.Journal of Quaternary Science, v. 27, no. 6, p. 639-648.

Newby, P.E., Killoran, P., Waldorf, M.R., Shuman, B.N., Webb, R.S., and Webb III, T., 2000, 14,000 Years of Sediment, Vegetation, and Water-Level Changes at the Makepeace Cedar Swamp, Southeastern Massachusetts: Quaternary Research, v. 53, no. 3, p. 352-368.

Nicoulin, A., and Ouimet, W.B., 2013, River terraces, incision, and post-glacial landscape evolution in southern New England: Abstracts with Programs - Geological Society of America, v. 45, no. 1, p. 99.

Noren, A.J., Bierman, P.R., and Galster, J.C., 2001, A 13,000-year regional record of Holocene storms from terrigenous lake sediment, northeastern USA: Abstracts with Programs - Geological Society of America, v. 33, no. 1, p. 57.

Noren, A.J., Bierman, P.R., Steig, E.J., Lini, A., and Southon, J., 2002, Millennial-scale storminess variability in the northeastern United States during the Holocene epoch: Nature (London), v. 419, no. 6909, p. 821-824.

Oswald, W.W., Foster, D.R., Doughty, E.D., and Faison, E.K., 2009, A record of Lateglacial and early Holocene environmental and ecological change from southwestern Connecticut, USA: Journal of Quaternary Science, v. 24, no. 6, p. 553-556.

Parris, A.S., Bierman, P.R., Noren, A.J., Prins, M.A., and Lini, A., 2010, Holocene paleostorms identified by particle size signatures in lake sediments from the Northeastern United States: Journal of Paleolimnology, v. 43, no. 1, p. 29-49.

Parris, A.S., Bosley, A., Noren, A., Bierman, P.R., Lini, A., and Ryan, P., 2002, Holocene flood frequency in New England; large, episodic events in the sediment record: Abstracts with Programs - Geological Society of America, v. 34, no. 6, p. 291.

Patton, P.C., 1988, Geomorphic response of streams to floods in the glaciated terrain of southern New England: New York, NY, United States (USA), John Wiley & Sons, New York, NY.

Patton, P.C., Burnett, A.W., Handsman, R.G., Wright, T.O., and Medlin, J.H., 1982, Processes of flood plain sedimentation and Holocene terrace formation, Housatonic River Basin, western Connecticut: Abstracts with Programs - Geological Society of America, v. 14, no. 1-2, p. 72.

Patton, P.C., and Handsman, R.G., 1984, Paleoflood record for the Housatonic River basin, western Connecticut: EOS, Transactions, American Geophysical Union, v. 65, no. 45, p. 891.

Phillips, S.P., Morris, T.H., Tingey, D.G., Eggett, D.L., and Zhou, W., 2015, Discriminant Analysis of Elemental Data To Differentiate Formations of Like Facies Vertically Across An Unconformity and Laterally Across A Paleotopographic Divide: Journal of Sedimentary Research, v. 85, no. 11, p. 1293-1309.

Pye, K., 1994, Sediment Transport and Depositional Processes: Cambridge, MA, Blackwell Scientific Publications, 384 p.

Ritch, N., and Hubeny, J.B., 2008, Analysis of core sediments gathered from Sluice Pond (Llynn, MA) indicate post-glacial environmental changes: Abstracts with Programs - Geological Society of America, v. 40, no. 2, p. 32.

Shuman, B., and Donnelly, J.P., 2006, The influence of seasonal precipitation and temperature regimes on lake levels in the northeastern United States during the Holocene: Quaternary Research, v. 65, no. 1, p. 44-56.

Stone, J.R., Schafer, J.P., London, E.H., DiGiacomo-Cohen, M.L., Lewis, R.S., Thompson, W.B., and Stone, B.D., 2005, Quaternary geologic map of Connecticut and Long Island Sound basin; with a section on sedimentary facies and morphosequences of glacial meltwater deposits: United States (USA), U. S. Geological Survey, 72, 2 sheets p.

Thorson, R.M., and Schile, C.A., 1995, Deglacial eolian regimes in New England: Bulletin of the Geological Society of America, v. 107, no. 7, p. 751-761.

Toonen, W.H.J., Winkels, T.G., Cohen, K.M., Prins, M.A., and Middelkoop, H., 2015, Lower Rhine historical flood magnitudes of the last 450 years reproduced from grain-size measurements of flood deposits using End Member Modelling: Catena, v. 130, p. 69-81.

USGS, 2014-12-10 13:18:08 EST, USGS Surface-Water Data for the Nation: http://waterdata.usgs.gov/nwis/sw (2014-12-2 2014).

Wang, R., Zhang, Y., Wünnemann, B., et al., 2015, Linkages between Quaternary climate change and sedimentary processes in Hala Lake, northern Tibetan Plateau, China: Journal of Asian Earth Sciences, v. 107, p. 140-150.

Whitney, G.G., 1994, From coastal wilderness to fruited plain: a history of environmental change in temperate North America from 1500 to the present: From coastal wilderness to fruited plain: a history of environmental change in temperate North America from 1500 to the present.

Wilkinson, B.H., and McElroy, B.J., 2007, The impact of humans on continental erosion and sedimentation: Bulletin of the Geological Society of America, v. 119, no. 1, p. 140-156.

Woodruff, J.D., Kratz, L., Yellen, B., and Martini, A., 2012, Tidal controls on the trapping of Hurricane Irene sediments in the lower Connecticut River: Ocean Sciences Meeting, v. 2012, p. 505.

Yellen, B., Woodruff, J.D., Kratz, L.N., Mabee, S.B., Morrison, J., and Martini, A.M., 2014, Source, conveyance and fate of suspended sediments following Hurricane Irene. New England, USA: Geomorphology, v. 226, p. 124-134.

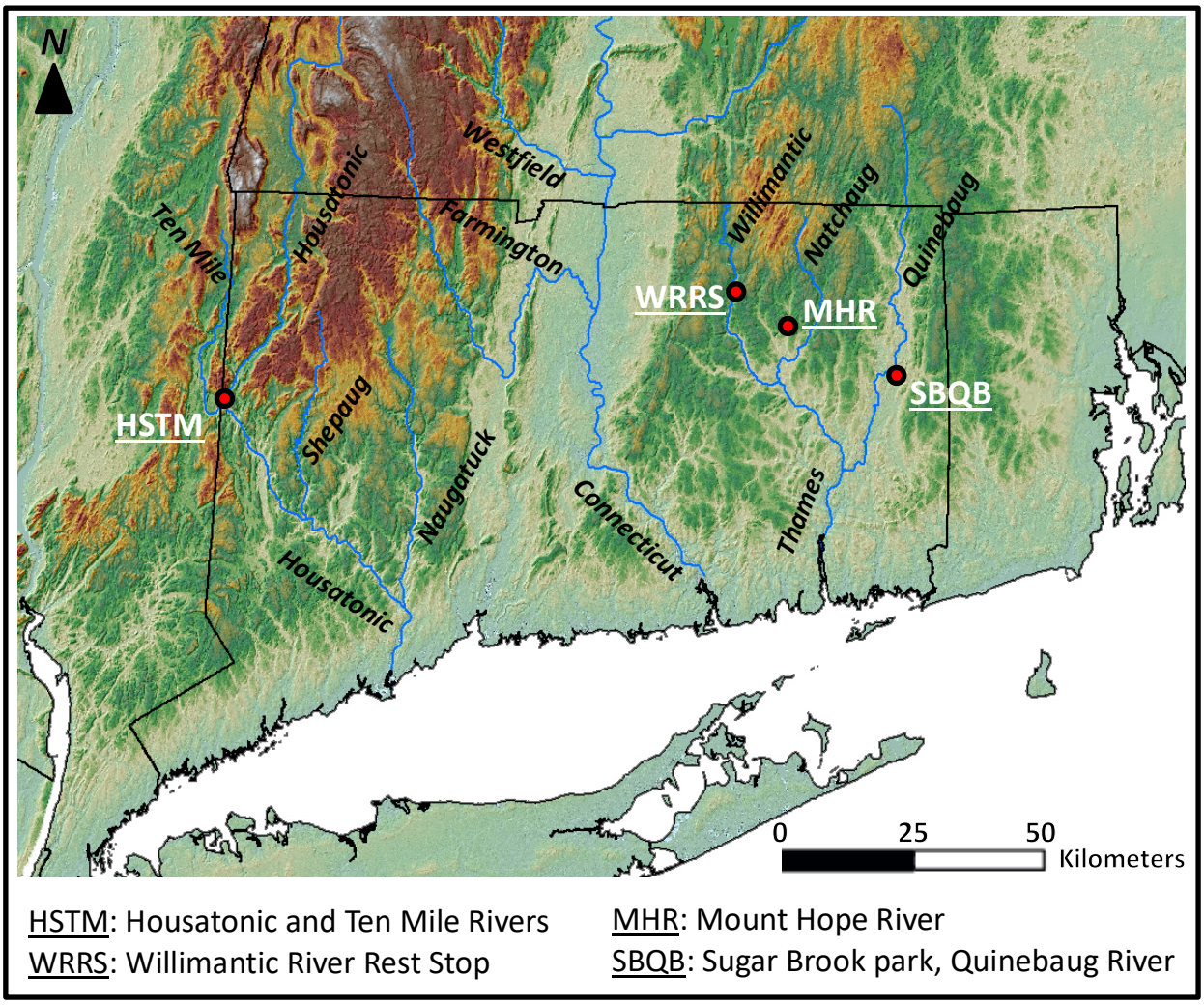

Figure 1. Field Site Locations: Field site locations across southern New England. The three major river drainages of Connecticut shown, the Housatonic River, Thames River, and Connecticut River and the major tributaries of those rivers. States shown are New York, Connecticut, Rhode Island, and Massachusetts.

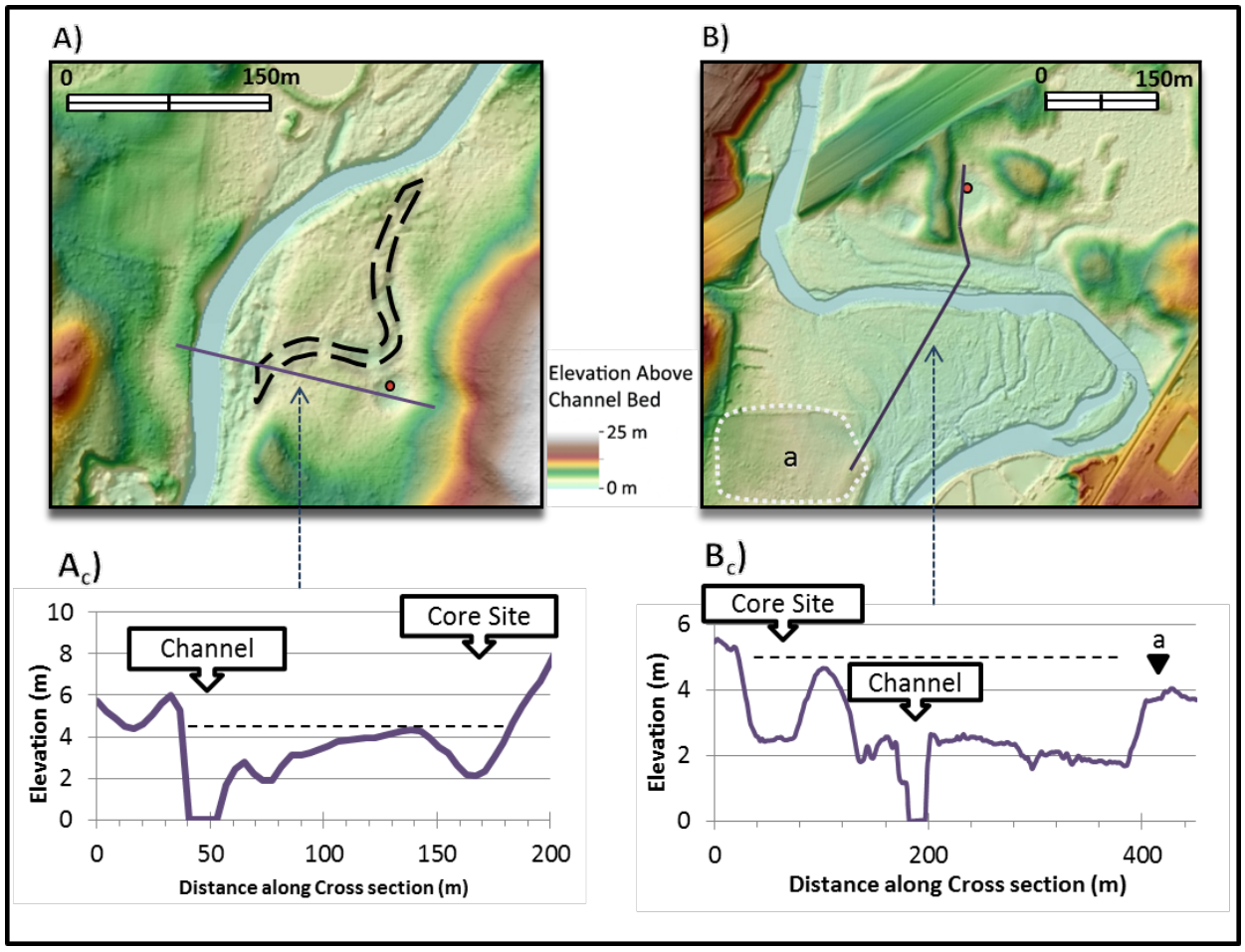

Figure 2 MHR and WRRS Field Site: 1 m LiDAR DEMs of the Mount Hope River (MHR, top left, A) and Willimantic River Rest Stop (WRRS, top right, B) field sites. The core sites are marked by the red point, the kettles of both sites are stereotypical circular depressions. In both field site insets the rivers flow from North to South. In A) the dashed black line marks the extent of a paleo-channel of the Mount Hope River. A terrace marked as *a* in near the WRRS core site. A_c and B_c are cross sections of the respective river indicated by the dashed arrow and the line of the cross section in A and B. The dashed line on each cross section highlights the depth to inundate the kettle site.

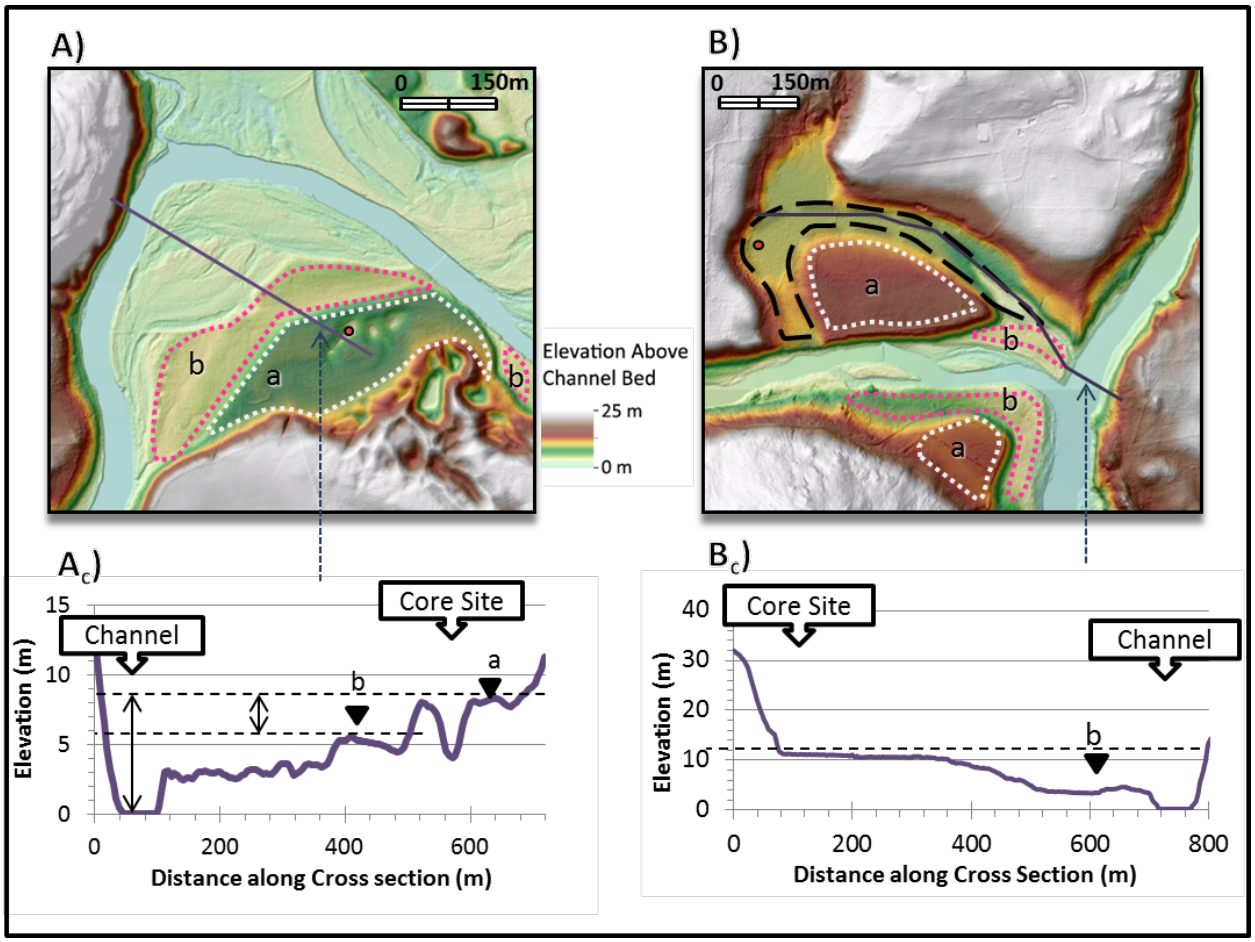

Figure 3 SBQB and HSTM Field Sites: 1m LiDAR DEM of the Quinebaug River at Sugar Brook Park (SBQB, top left, A), and Housatonic and Ten Mile River (HSTM, top right, B) field sites. Core locations are marked by red dots. In A the Quinebaug River flows from East to West. In B the Housatonic River flows from North to South and the Ten Mile River flows into the Housatonic from the West. The thick black dashed line in the HSTM LiDAR denotes the interpreted paleo-channel path of the Housatonic River. A_c and B_c are cross sections of the respective river indicated by the dashed arrow and the line of the cross section in A and B. The dashed line on each cross section highlights the depth to inundate the kettle site. Dashed white and pink outline the terraces identified at each field site. The higher terrace is terrace a and the lower terrace is *b*, these are also indicated in the cross sections when the section path traverses the terrace.

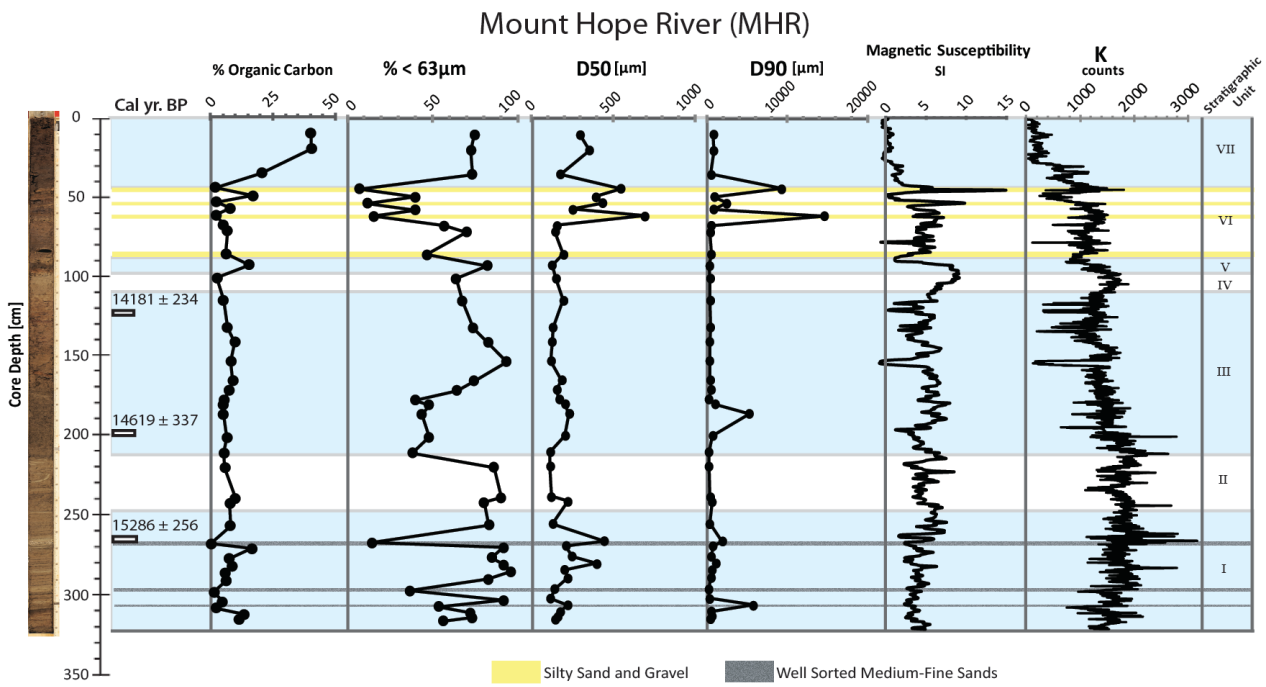

Figure 4. Mount Hope Core Data: Calibrated ages at marked depths, LOI results presented as % Organic Carbon, % of sample finer than 63 micron, D50 and D90 percent by weight given in grain size of measured material. Visible event deposits marked by bars coinciding with composition of observed material. K and MS drop at 164 cm due to large woody debris.

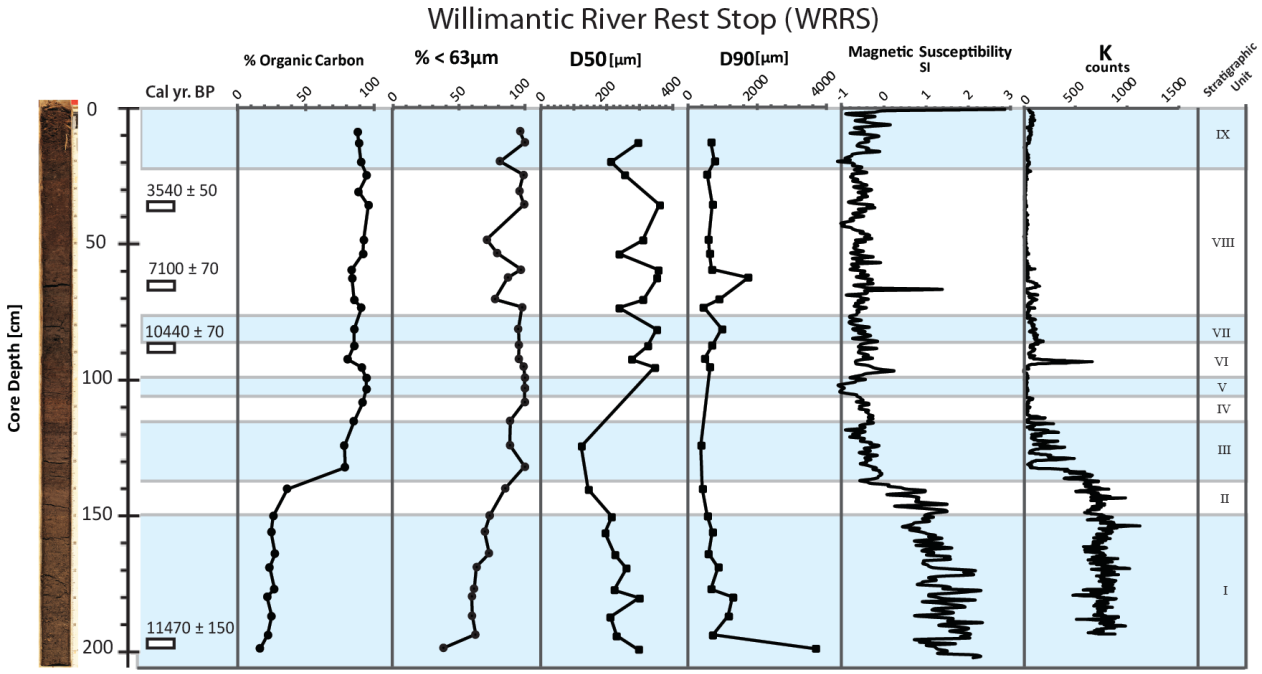

Figure 5. Willimantic River Rest Stop Core Data: Calibrated ages at marked depths, LOI results presented as % Organic Carbon, % of sample finer than 63 micron, D50 and D90 percent by weight given in grain size of measured material.

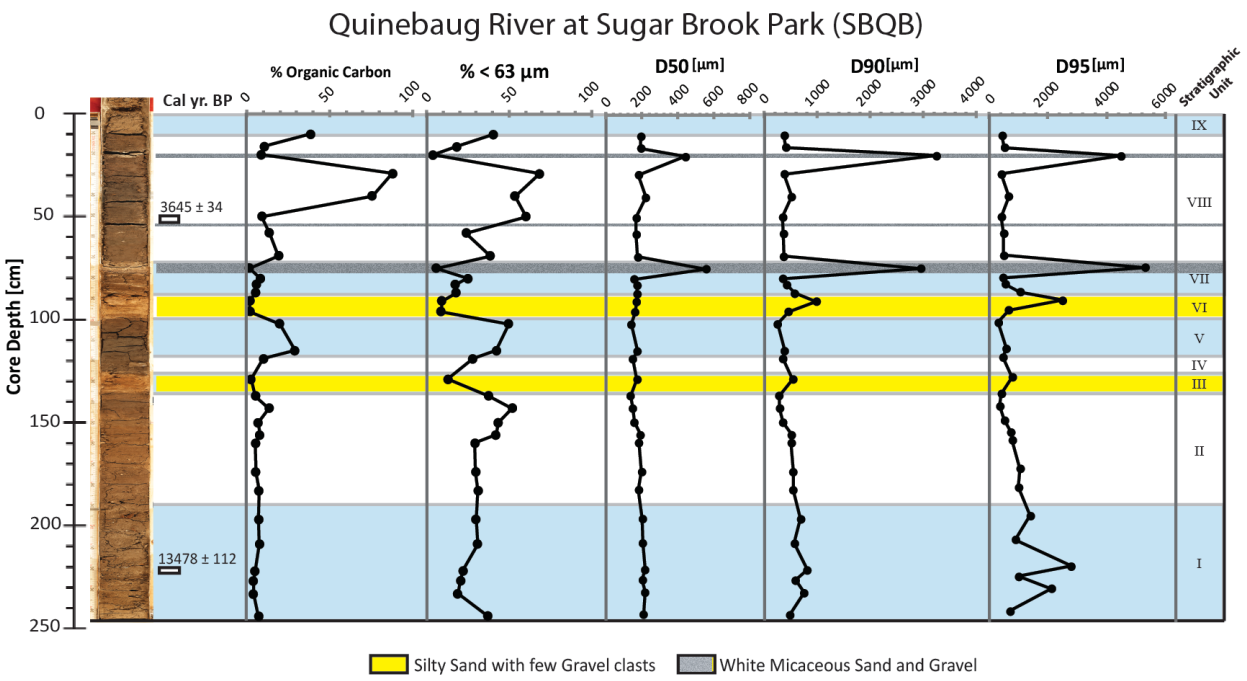

Figure 6. Quinebaug Core Data: Calibrated ages at marked depths, LOI results presented as % Organic Carbon, % of sample finer than 63 micron, D50 and D90 percent by weight given in grain size of measured material. Visible event deposits marked by bars coinciding with composition of observed material.

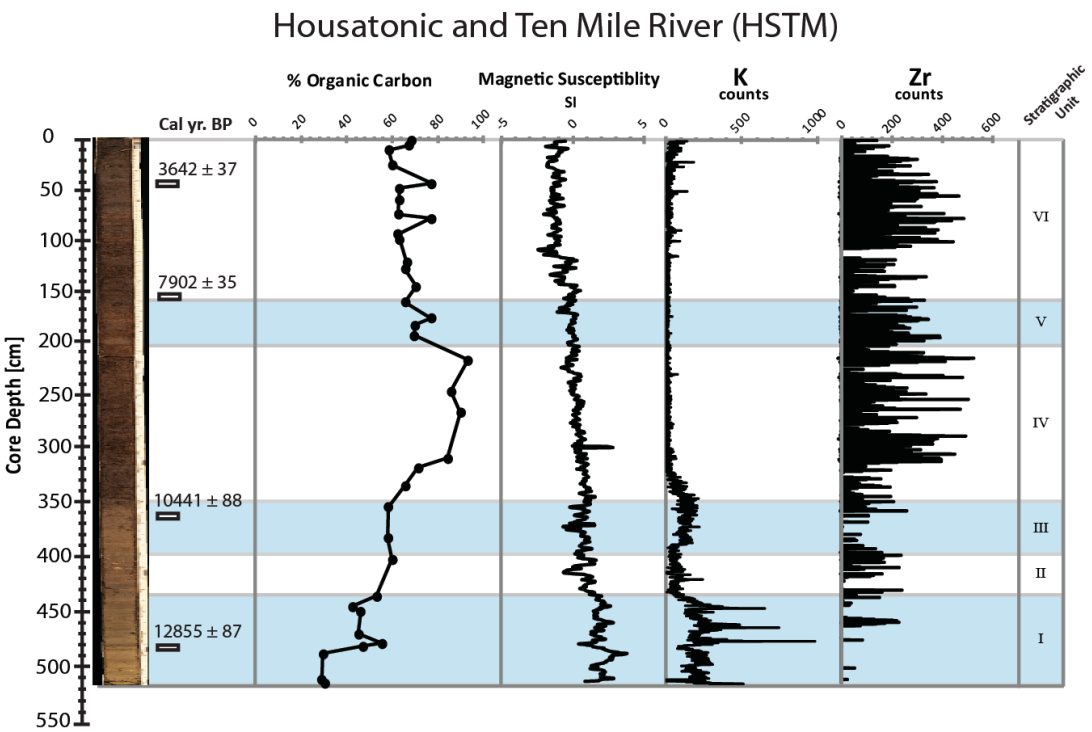

Figure 7. Housatonic and Ten Mile River Core Data: Housatonic and Ten Mile River, HSTM, Calibrated ages at marked depths, LOI results presented as % Organic Carbon. The K signal reduction in unit II, coinciding with abundant animal shells, suggests a period with a more stable lake with reduced sediment input between higher sediment input lacustrine settings. Zr counts increase and K decrease ~308 cm depth. Grain size measurements were not performed on core samples.

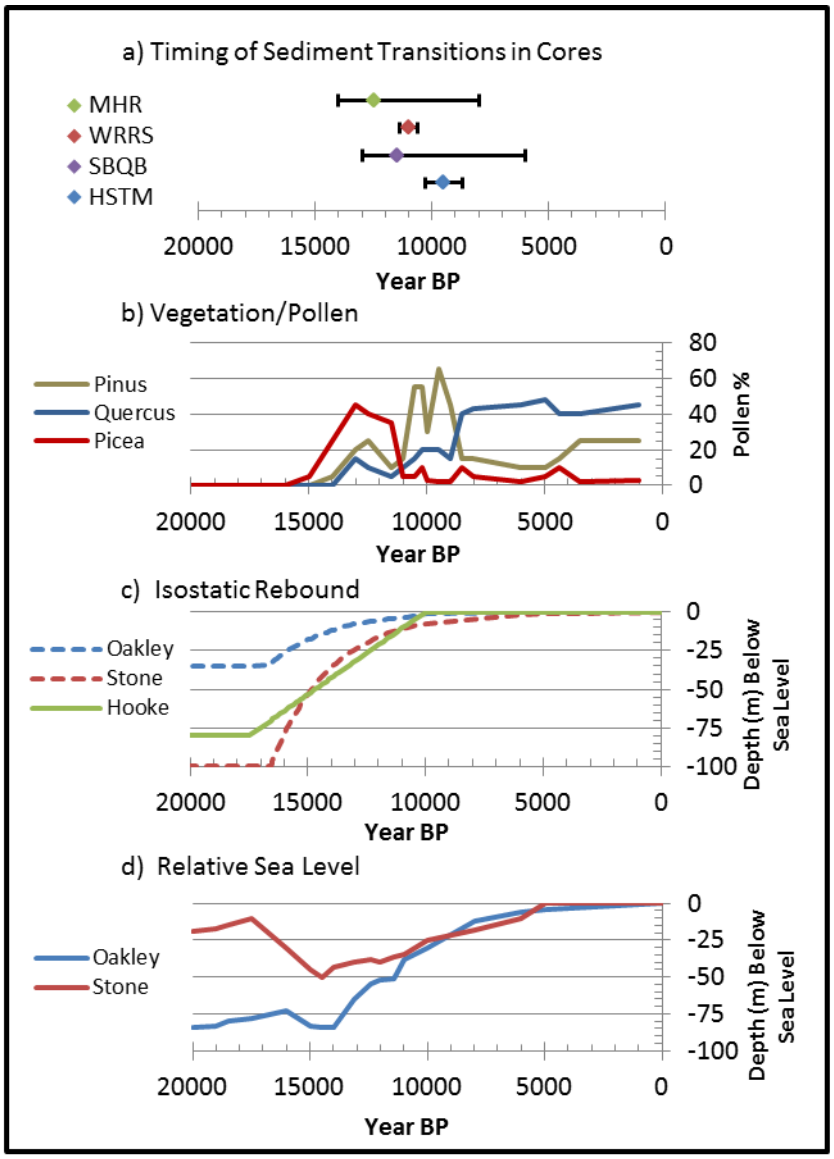

Figure 8. Projected Periods of Erosion with Vegetation, Rebound, and Relative Sea Level: a) estimated timing of sediment transitions from each core with error bars denoting date range. Lower age limit of transition for MHR and SBQB comes from radiometric dates, upper age extent for both cores are an estimate. Timing range for HSTM and WRRS are directly from radiometric dates above and below sediment transition. Pollen records modified from Davis, 1983; Menking et al., 2012; and Oswald et al., 2009. Data from sampled studies recorded % pollen of total pollen counted. Graphs c and d mod Oakley and Boothroyd, 2012; Stone, 2005; Hooke et al., 1993. Hooke interpreted linear rebound Oakely and Stone used rebound with a half-life of 1750 yr but disagree on magnitude, hence the differing relative sea level. Stone reported relative sea level for Long Island Sound, Oakley presented relative sea level for Block Island.

Table 1: Radiocarbon Dated Core Material

Core	Sample Depth	Material	Mass	Uncalibrated Age year BP	Error	Calibrated Age year BP	Error
MHR	125	Wood Fibers	0.47 g	12150	55	14181	234
MHR	200	Wood, Twig	0.03 g	12400	55	14619	337
MHR	266	Wood Fibers	0.30 g	12800	60	15286	256
WRRS	36	Ragweed	---	-----	---	3540	50
WRRS	65	Peat Fibers	---	-----	---	7100	70
WRRS	90	Wood Fibers	---	-----	---	10440	70
WRRS	198	Wood Fibers	---	-----	---	11470	150
SBQB	53	Wood Fibers	0.65 g	3390	20	3645	34
SBQB	227	Wood Fibers	0.23 g	1160	45	13478	112
HSTM	44	Wood Fibers	0.06 g	3390	25	3642	37
HSTM	156	Wood Fibers	0.28 g	7060	35	7902	35
HSTM	363	Woody Bark	0.38 g	9270	50	10441	88
HSTM	482	Wood, Twig	0.10 g	10900	65	12855	87

Radiocarbon dates acquired from NOSAMS Facility at Woods Hole Oceanographic Institute, Massachusetts for cores MHR, HSTM, and SBQB. WRRS core dates reported in Bugden, 1994 did not record mass or uncalibrated age.

Table 2: Flood Estimation Widths, Depths, Channel Roughness, and Velocity

		Mean Depth (m)	Width (m)	Slope	roughness coeficient	Depth Average Velocity (m/s)
Core Site						**MANNING**
MHR		4	41.5	0.002	0.065	1.7
MHR		4	41.5	0.002	0.11	1.0
MHR		4	135	0.002	0.065	1.7
MHR		4	135	0.002	0.11	1.0
WRRS		4.7	98.4	0.002	0.065	1.9
WRRS		4.7	98.4	0.002	0.11	1.1
WRRS		4.7	131	0.002	0.065	1.9
WRRS		4.7	131	0.002	0.11	1.1
SBQB		8.35	170	0.0009	0.065	1.9
SBQB		8.35	170	0.0009	0.11	1.1
SBQB		8.35	593	0.0009	0.065	1.9
SBQB		8.35	593	0.0009	0.11	1.1
SBQB Terrace b		4.1	170	0.0009	0.065	1.2
SBQB Terrace b		4.1	170	0.0009	0.11	0.7
SBQB Terrace b		4.1	593	0.0009	0.065	1.2
SBQB Terrace b		4.1	593	0.0009	0.11	0.7
HSTM		10.5	115	0.004	0.065	4.7
HSTM		10.5	115	0.004	0.11	2.8
HSTM		10.5	160	0.004	0.065	4.7
HSTM		10.5	160	0.004	0.11	2.8
Core	**Sample Depth (cm)**					**DEITRICH**
MHR	44	4	----	----	----	4.7
MHR	53	4	----	----	----	3.66
MHR	61	4	----	----	----	5.99
MHR	265	4	----	----	----	3.75
WRRS	54	4.7	----	----	----	1.67
WRRS	74	4.7	----	----	----	2.4
WRRS	93	4.7	----	----	----	2.54
SBQB	20	8.35	----	----	----	3.7
SBQB	75	8.35	----	----	----	4.79
SBQB	91	8.35	----	----	----	1.03
SBQB	129	8.35	----	----	----	1.04

Table 3: Estimated Flood Recurrence Intervals

Site / Core name with Sample Depth	Recurrence Interval Small Width	Recurrence Interval Large Width
MHR Manning n=0.065	14188	$6.81*10^{13}$
MHR Manning n=0.11	248	$1.30*10^{8}$
MHR 44	$3.19*10^{11}$	$5.60*10^{37}$
MHR 53	$8.44*10^{8}$	$2.31*10^{29}$
MHR 61	$5.02*10^{14}$	$1.41*10^{48}$
MHR 265	$1.41*10^{9}$	$1.23*10^{30}$
WRRS Manning n=0.065	22170	615472
WRRS Manning n=0.11	366	2608
WRRS 54	5726	101519
WRRS 74	254333	$1.58*10^{7}$
WRRS 93	526464	$4.17*10^{7}$
SBQB Manning n=0.065	$8.13*10^{6}$	$7.4*10^{24}$
SBQB Manning n=0.11	9064	$3.71*10^{14}$
SBQB 20	$5.63*10^{13}$	$5.39*10^{48}$
SBQB 75	$7.80*10^{17}$	$1.51*10^{63}$
SBQB 91	4035	$2.21*10^{13}$
SBQB 129	4404	$2.99*10^{13}$
SBQB Terrace n=0.065	79	$2.44*10^{7}$
SBQB Terrace n=0.11	10	17336
HSTM Manning n=0.065	$3.03*10^{27}$	$1.74*10^{38}$
HSTM Manning n=0.11	$1.72*10^{16}$	$3.90*10^{22}$

Calculated Recurrence intervals of floods which flood each field site to a depth of 0.5m based on the rating curve established by modern peak annual flow measurements. The SBQB Terrace b calculations model a flood from a river projected to be 1m below the elevation of terrace b as shown in Figure 4.

Appendix 1 MHR and WRRS K and Zr

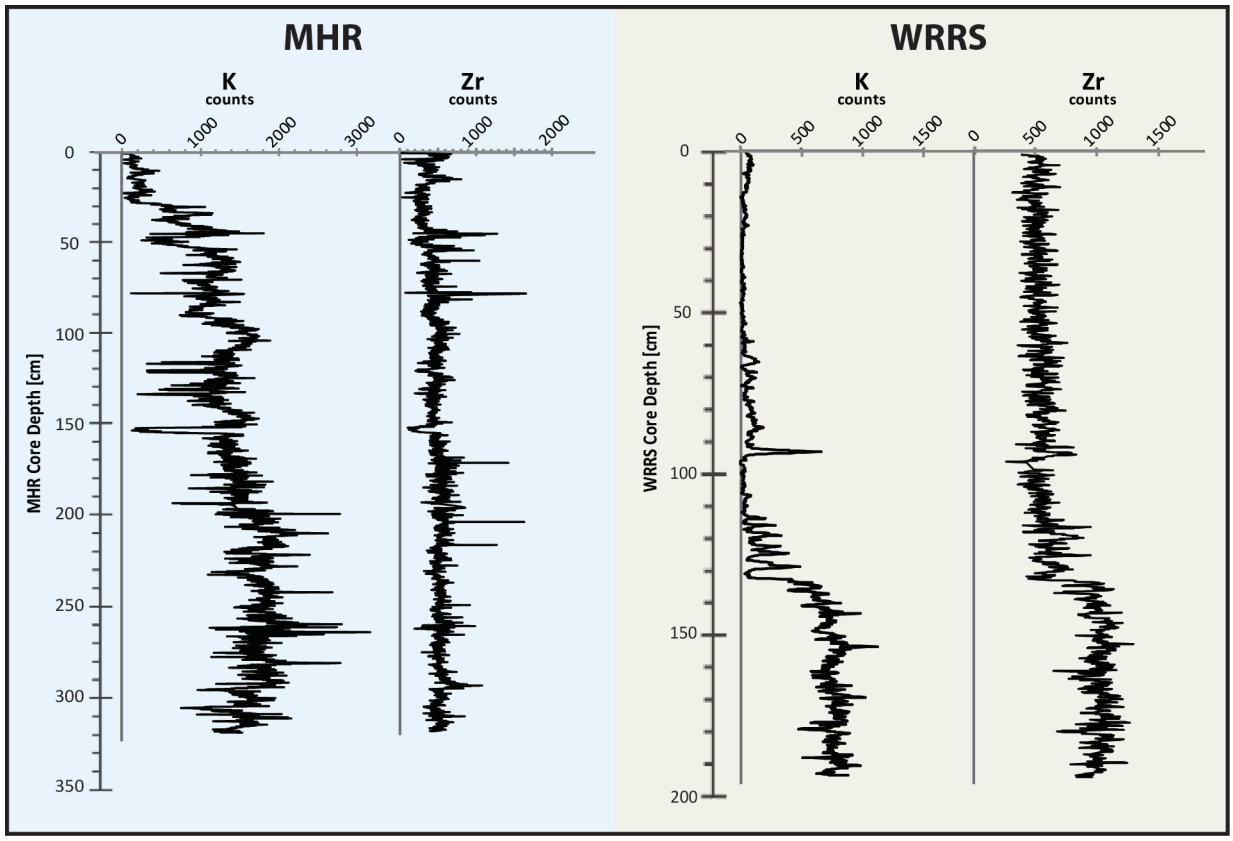

K and Zr counts for MHR and WRRS. MHR has very little Zr variability throughout the core. WRRS lower core has K and Zr counts near 1000 in the lower core while the upper core both decrease in counts with Zr maintain counts around 500 for the organic rich region of core.

Appendix 2 Expanded MHR Field site

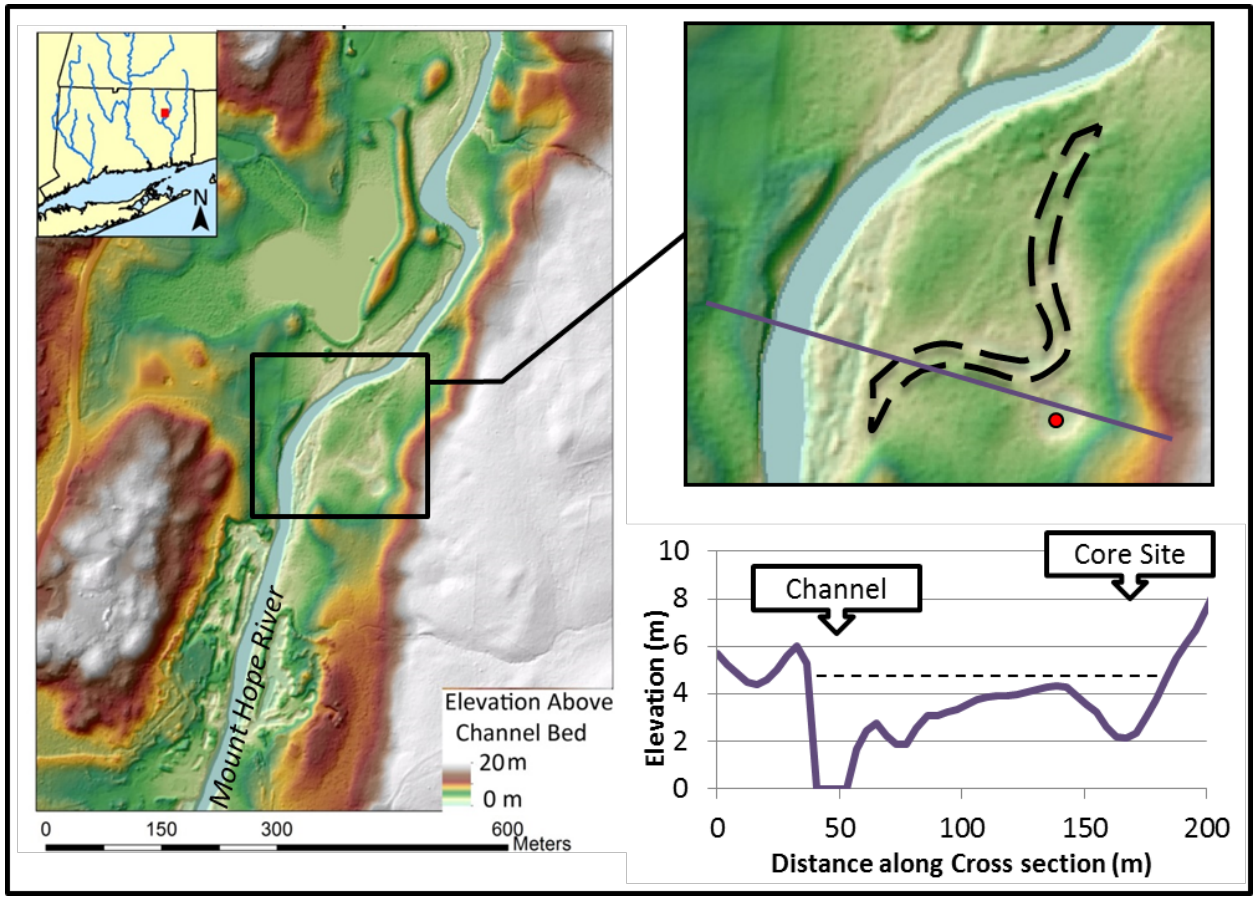

MHR Mount Hope River field site: *left* Local area DEM shaded by elevation above the nearest modern channel bed. *Upper right* field site zoom showing paleo-channel with dashed black line sample site denoted with red dot. Dark purple line indicates cross-section. *Lower right* cross section with black dashed line showing minimum depth to flood the kettle.

Appendix 3 Expanded WRRS Field site

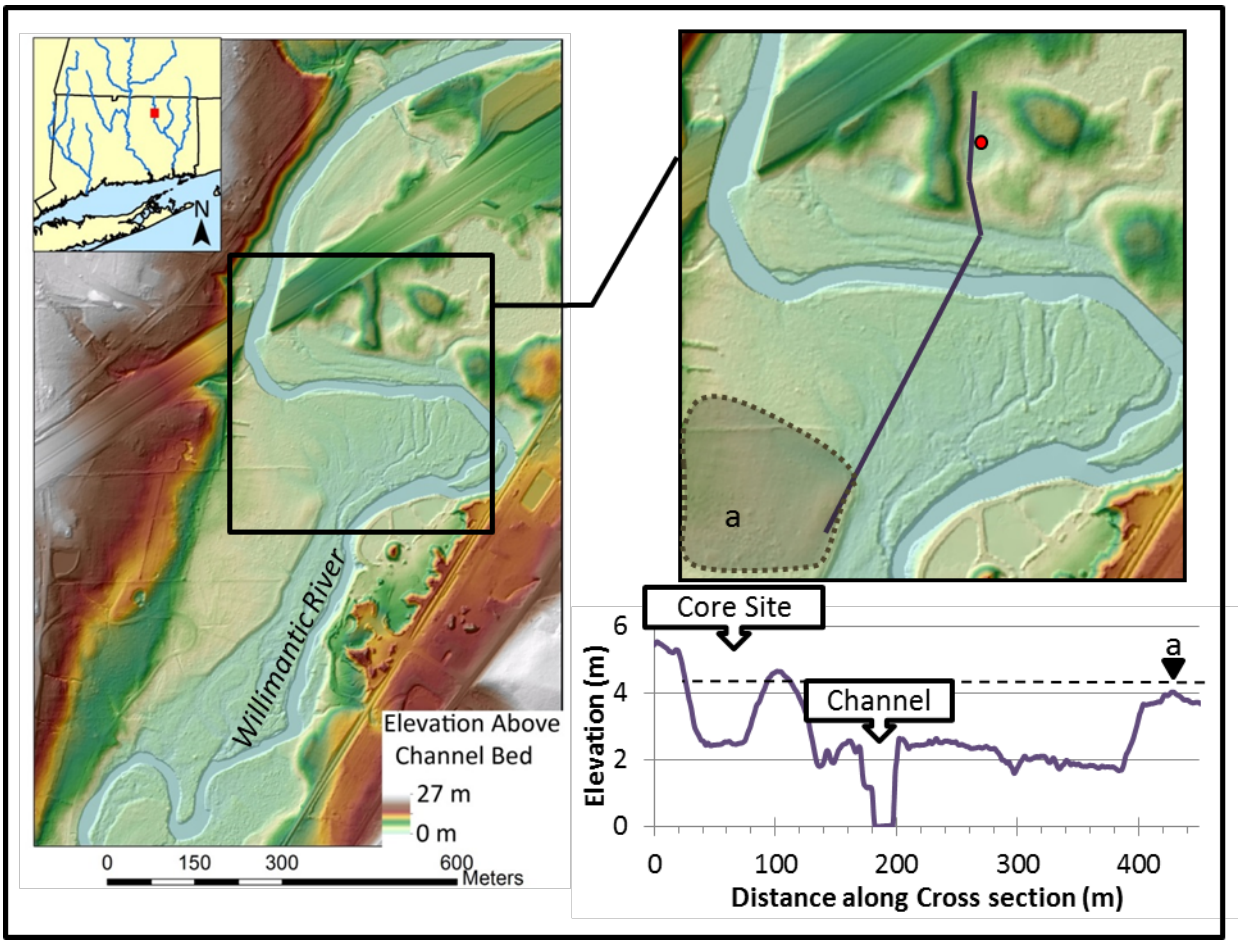

WRRS Willimantic River Rest Stop field site: *left* Local area DEM colored based on elevation above the nearest modern channel bed core of field site with upper left inset of site location in CT and major rivers. Route 84 cuts diagonally across the area *upper right* showing cross-section and coring site (red circle). Terrace feature highlighted in shape **a** *lower right* cross section indicated in above inset, terrace **a** has an average elevation of 4m above channel bed. The dashed line indicates the topographic lip separating the sampled kettle from the modern channel, elevation 4.4m.

Appendix 4 Expanded SBQB Field Site

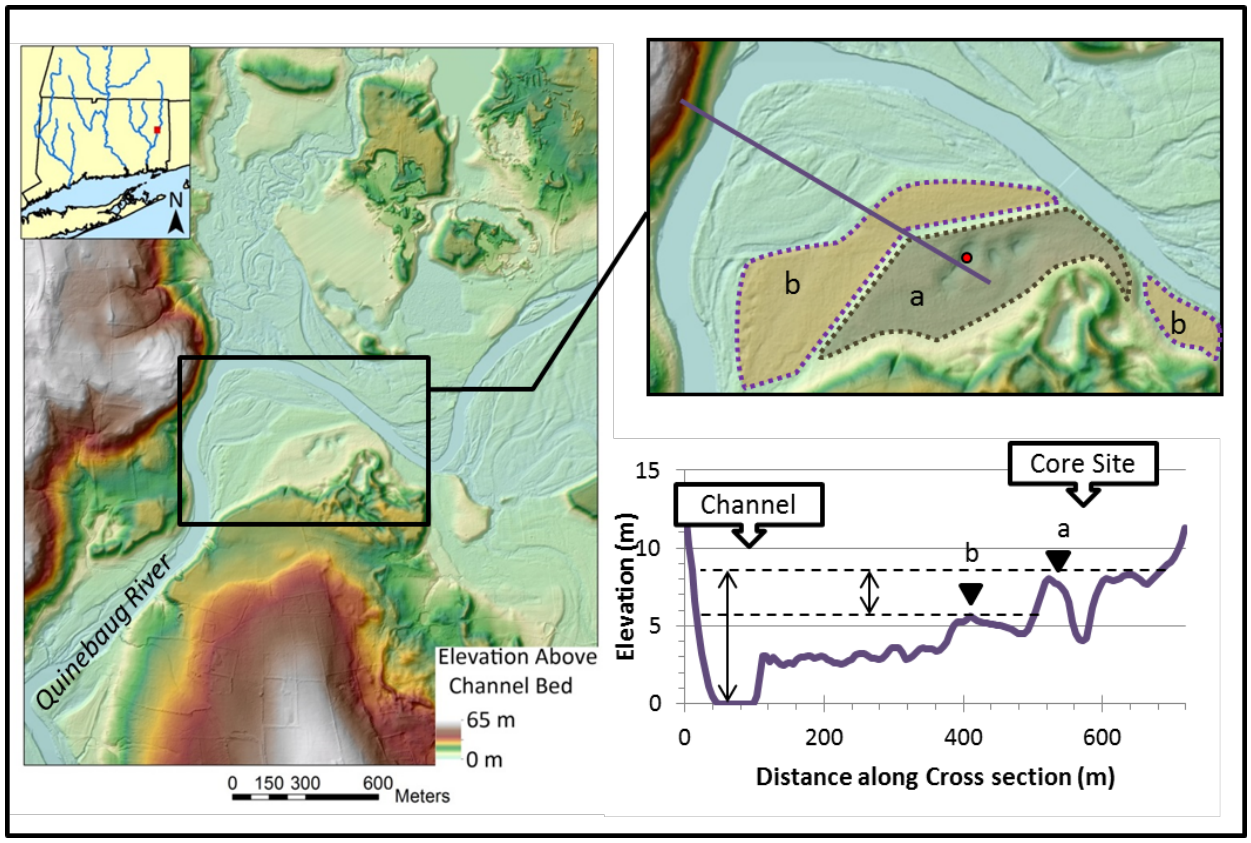

SBQB Quinebaug River at Sugar Brook Park Field Site: *left* Local area DEM colored based on elevation above the nearest modern channel bed core of field site with upper left inset of site location in CT and major rivers, site at center in inset is 38m above sea level, the Quinebaug river flows from right to left *upper right* showing cross-section and coring site (red circle). Two terraces, **a** and **b**, are highlighted *lower right* cross section indicated in above inset, terrace **a** has an average elevation of 8m above channel bed, terrace **b** has maximum elevation above channel bed of 5.5m and slopes toward terrace **a** where the elevation is 4.4m.

Appendix 5 Expanded HSTM Field Site

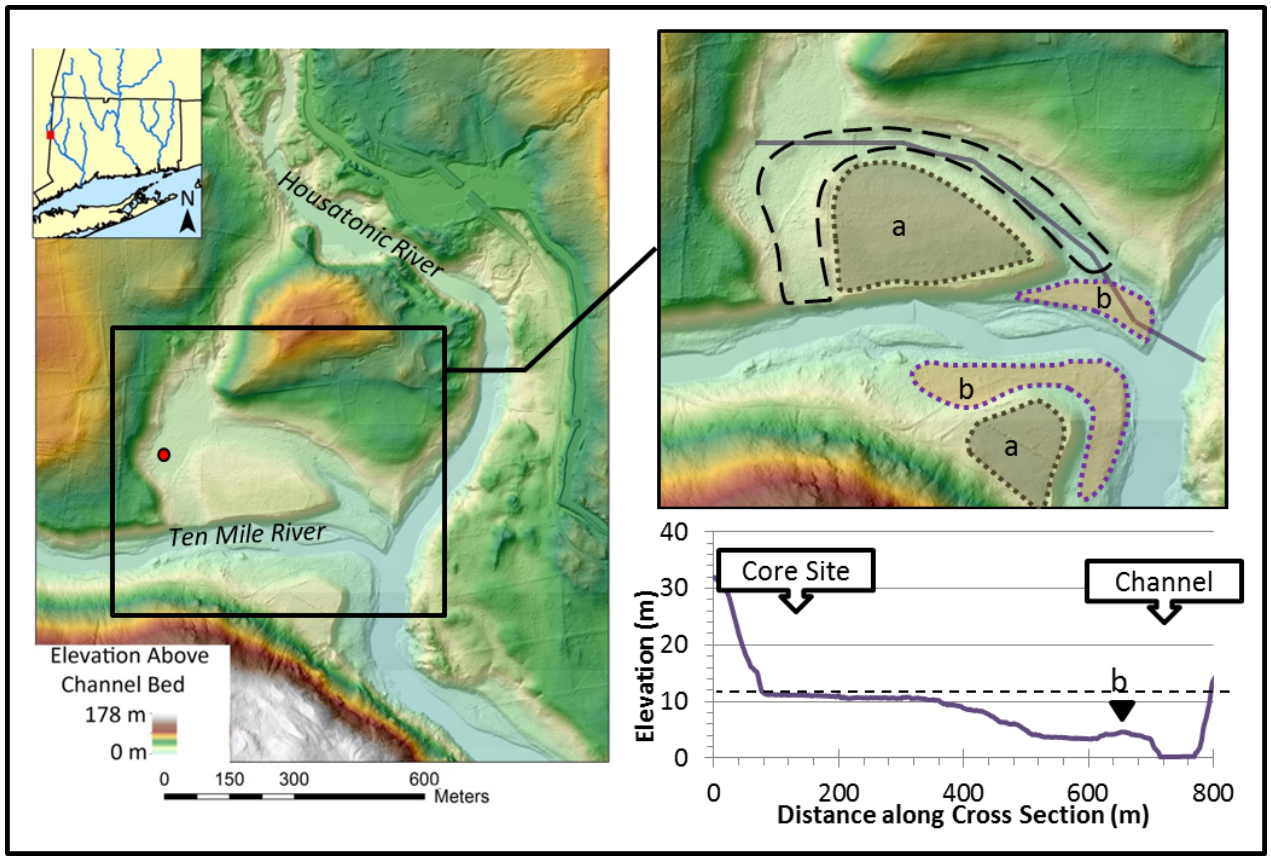

HSTM Housatonic and Ten Mile River Field Site: *left* Local area DEM colored based on elevation above the nearest modern channel bed core of field site with upper left inset of site location in CT and major rivers. Core site indicated by red circle, 93m above sea level. The Ten Mile River flows in from left to right, Housatonic River flows from top to bottom *upper right* inset showing cross-section and incisional features. Two terraces, **a** and **b**, are highlighted. Terrace **a** has an average elevation 13m above the adjacent river, lower terrace **b** is average 4.5m above the river bed. Shape outlined by a black dashed line is interpreted abandoned paleo-channel path of the Housatonic and/or Ten Mile River *lower right* cross section indicated in above inset following the paleo-channel down to a small marsh set behind terrace **b** then across the Housatonic River.

Appendix 6 Mount Hope Core Description

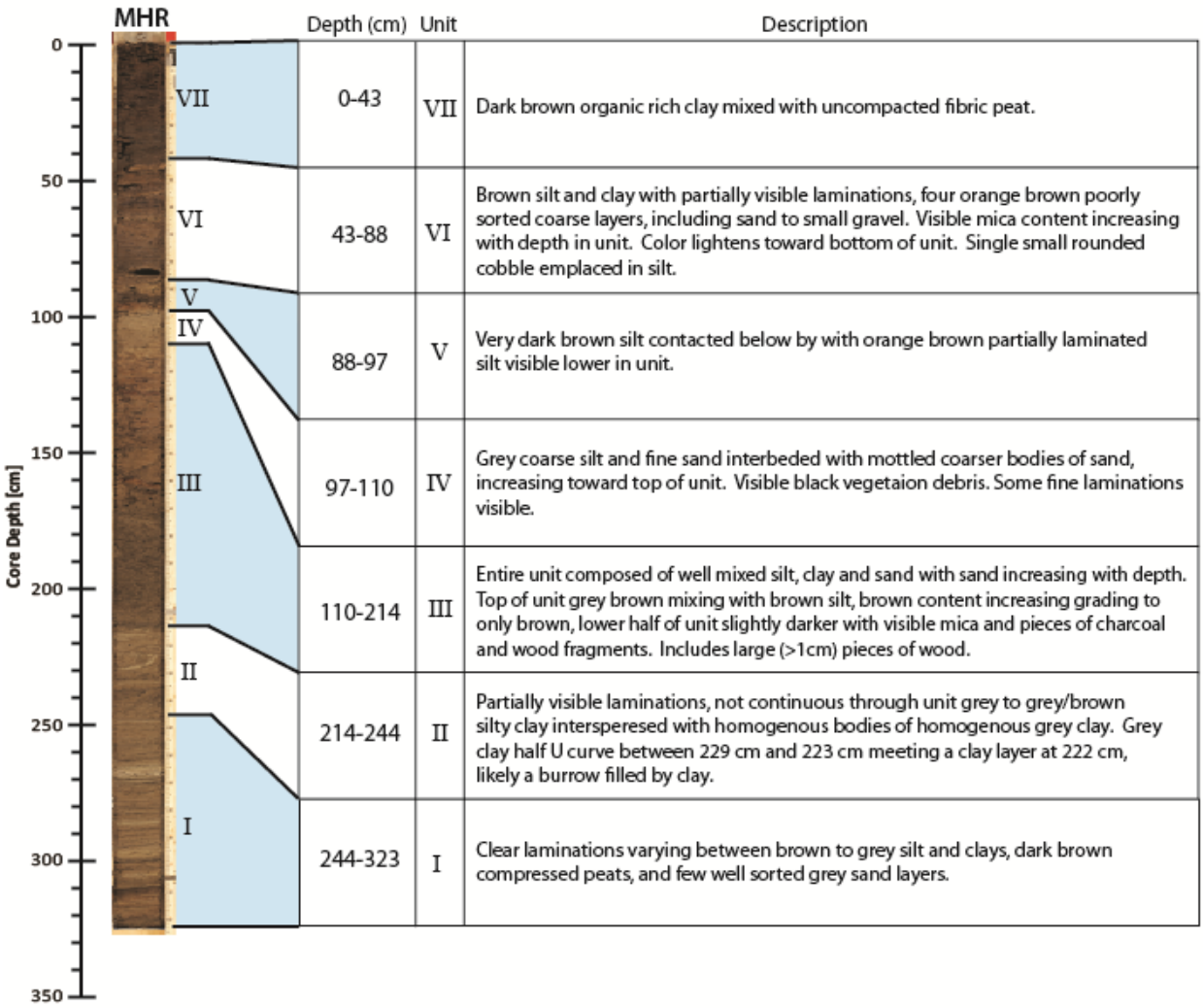

Depth (cm)	Unit	Description
0-43	VII	Dark brown organic rich clay mixed with uncompacted fibric peat.
43-88	VI	Brown silt and clay with partially visible laminations, four orange brown poorly sorted coarse layers, including sand to small gravel. Visible mica content increasing with depth in unit. Color lightens toward bottom of unit. Single small rounded cobble emplaced in silt.
88-97	V	Very dark brown silt contacted below by with orange brown partially laminated silt visible lower in unit.
97-110	IV	Grey coarse silt and fine sand interbeded with mottled coarser bodies of sand, increasing toward top of unit. Visible black vegetaion debris. Some fine laminations visible.
110-214	III	Entire unit composed of well mixed silt, clay and sand with sand increasing with depth. Top of unit grey brown mixing with brown silt, brown content increasing grading to only brown, lower half of unit slightly darker with visible mica and pieces of charcoal and wood fragments. Includes large (>1cm) pieces of wood.
214-244	II	Partially visible laminations, not continuous through unit grey to grey/brown silty clay intersperesed with homogenous bodies of homogenous grey clay. Grey clay half U curve between 229 cm and 223 cm meeting a clay layer at 222 cm, likely a burrow filled by clay.
244-323	I	Clear laminations varying between brown to grey silt and clays, dark brown compressed peats, and few well sorted grey sand layers.

Mount Hope River Core Description. On left is brightened compiled core photo taken after a 1 day drying period. Depth measured in compressed core depth.

Appendix 7 Willimantic Core Description

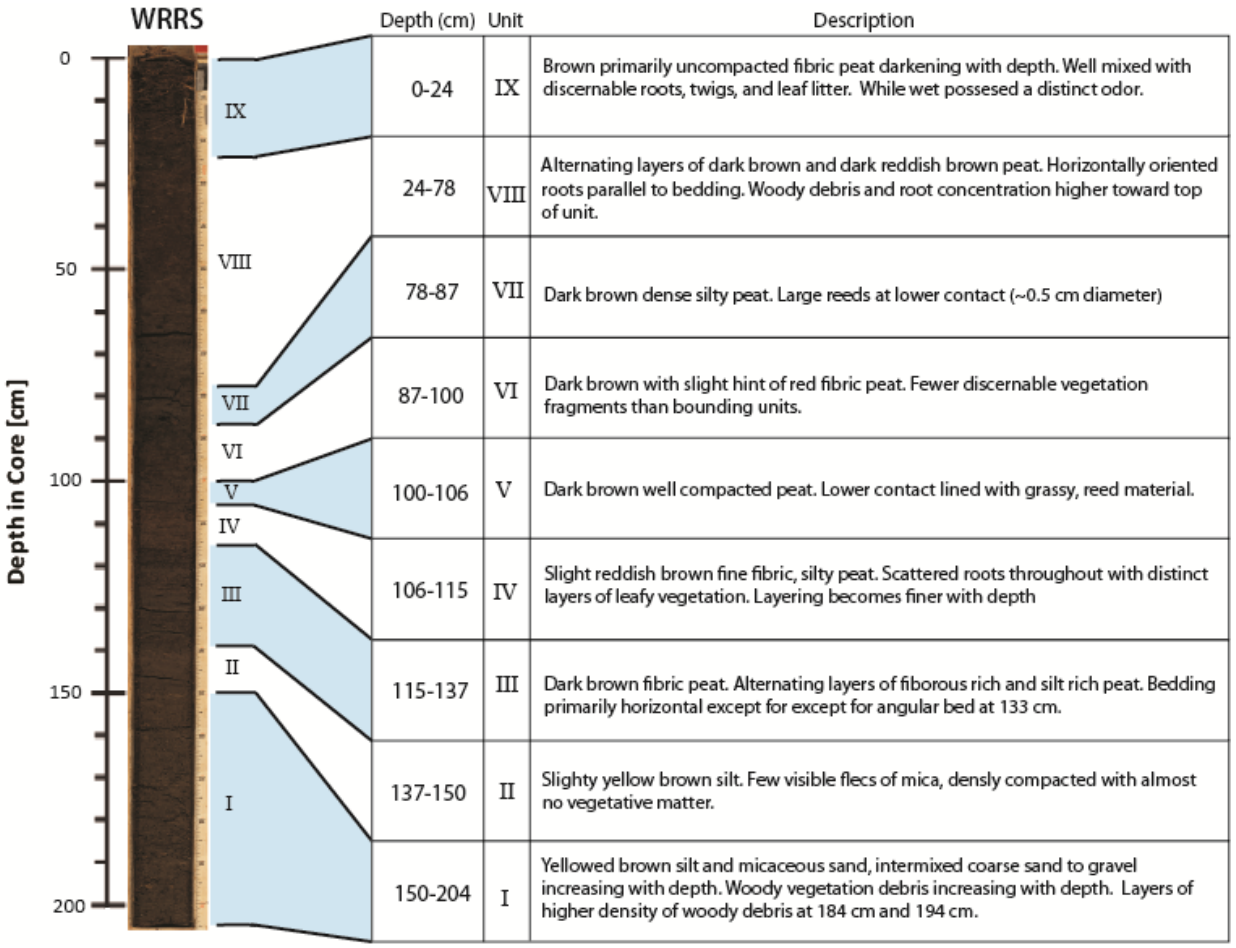

Depth (cm)	Unit	Description
0-24	IX	Brown primarily uncompacted fibric peat darkening with depth. Well mixed with discernable roots, twigs, and leaf litter. While wet possesed a distinct odor.
24-78	VIII	Alternating layers of dark brown and dark reddish brown peat. Horizontally oriented roots parallel to bedding. Woody debris and root concentration higher toward top of unit.
78-87	VII	Dark brown dense silty peat. Large reeds at lower contact (~0.5 cm diameter)
87-100	VI	Dark brown with slight hint of red fibric peat. Fewer discernable vegetation fragments than bounding units.
100-106	V	Dark brown well compacted peat. Lower contact lined with grassy, reed material.
106-115	IV	Slight reddish brown fine fibric, silty peat. Scattered roots throughout with distinct layers of leafy vegetation. Layering becomes finer with depth
115-137	III	Dark brown fibric peat. Alternating layers of fiborous rich and silt rich peat. Bedding primarily horizontal except for except for angular bed at 133 cm.
137-150	II	Slighty yellow brown silt. Few visible flecs of mica, densly compacted with almost no vegetative matter.
150-204	I	Yellowed brown silt and micaceous sand, intermixed coarse sand to gravel increasing with depth. Woody vegetation debris increasing with depth. Layers of higher density of woody debris at 184 cm and 194 cm.

Willimantic River Core Description. On left is brightened compiled core photo taken after a 1 day drying period. Depth measured in compressed core depth.

Appendix 8 Quinebaug Core Description

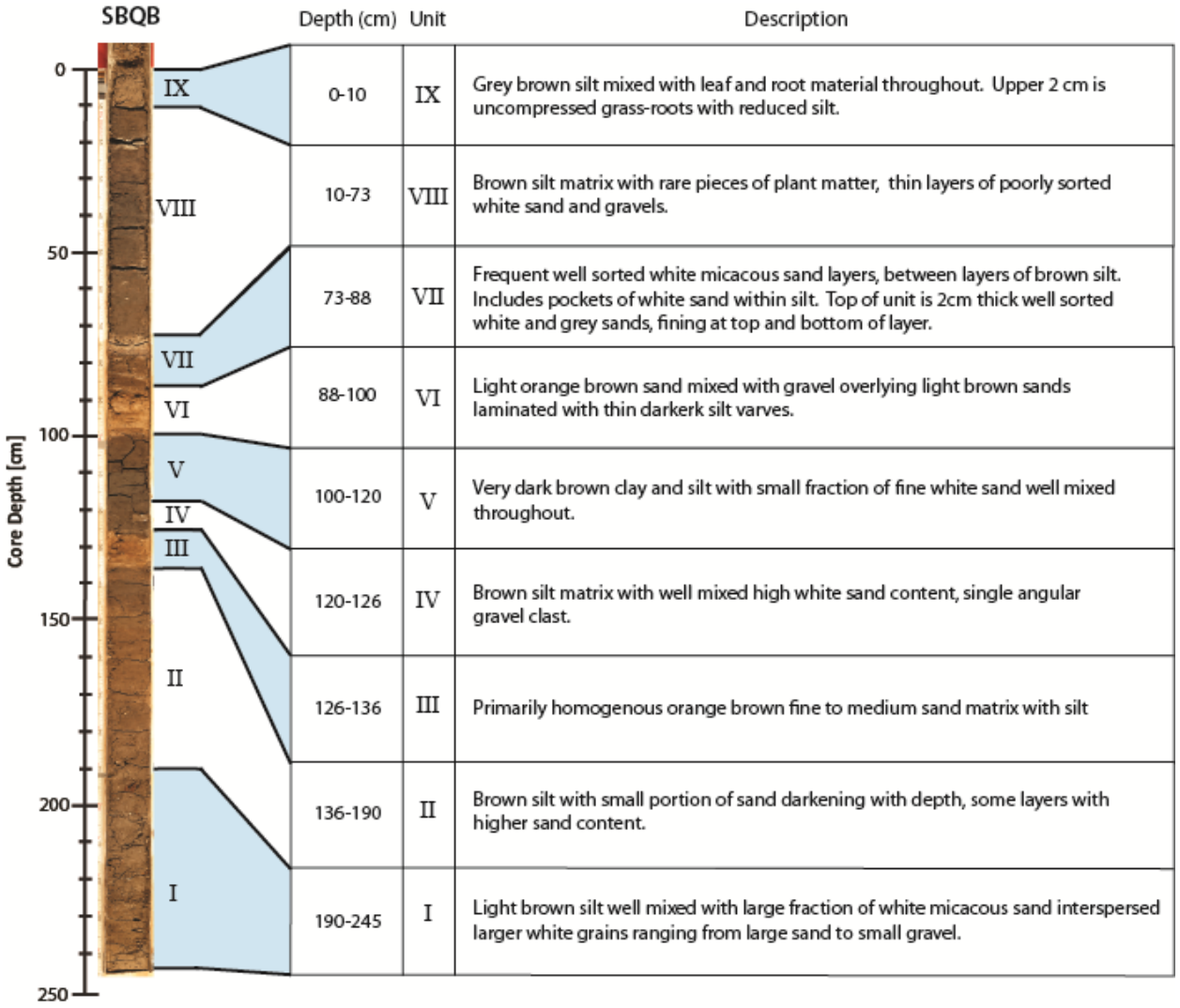

Depth (cm)	Unit	Description
0-10	IX	Grey brown silt mixed with leaf and root material throughout. Upper 2 cm is uncompressed grass-roots with reduced silt.
10-73	VIII	Brown silt matrix with rare pieces of plant matter, thin layers of poorly sorted white sand and gravels.
73-88	VII	Frequent well sorted white micacous sand layers, between layers of brown silt. Includes pockets of white sand within silt. Top of unit is 2cm thick well sorted white and grey sands, fining at top and bottom of layer.
88-100	VI	Light orange brown sand mixed with gravel overlying light brown sands laminated with thin darkerk silt varves.
100-120	V	Very dark brown clay and silt with small fraction of fine white sand well mixed throughout.
120-126	IV	Brown silt matrix with well mixed high white sand content, single angular gravel clast.
126-136	III	Primarily homogenous orange brown fine to medium sand matrix with silt
136-190	II	Brown silt with small portion of sand darkening with depth, some layers with higher sand content.
190-245	I	Light brown silt well mixed with large fraction of white micacous sand interspersed larger white grains ranging from large sand to small gravel.

Quinebaug River at Sugar Brook Park Core Description. On left is brightened compiled core photo taken after a 1 day drying period. Depth measured in compressed core depth.

Appendix 9 Housatonic and Ten Mile Core Description

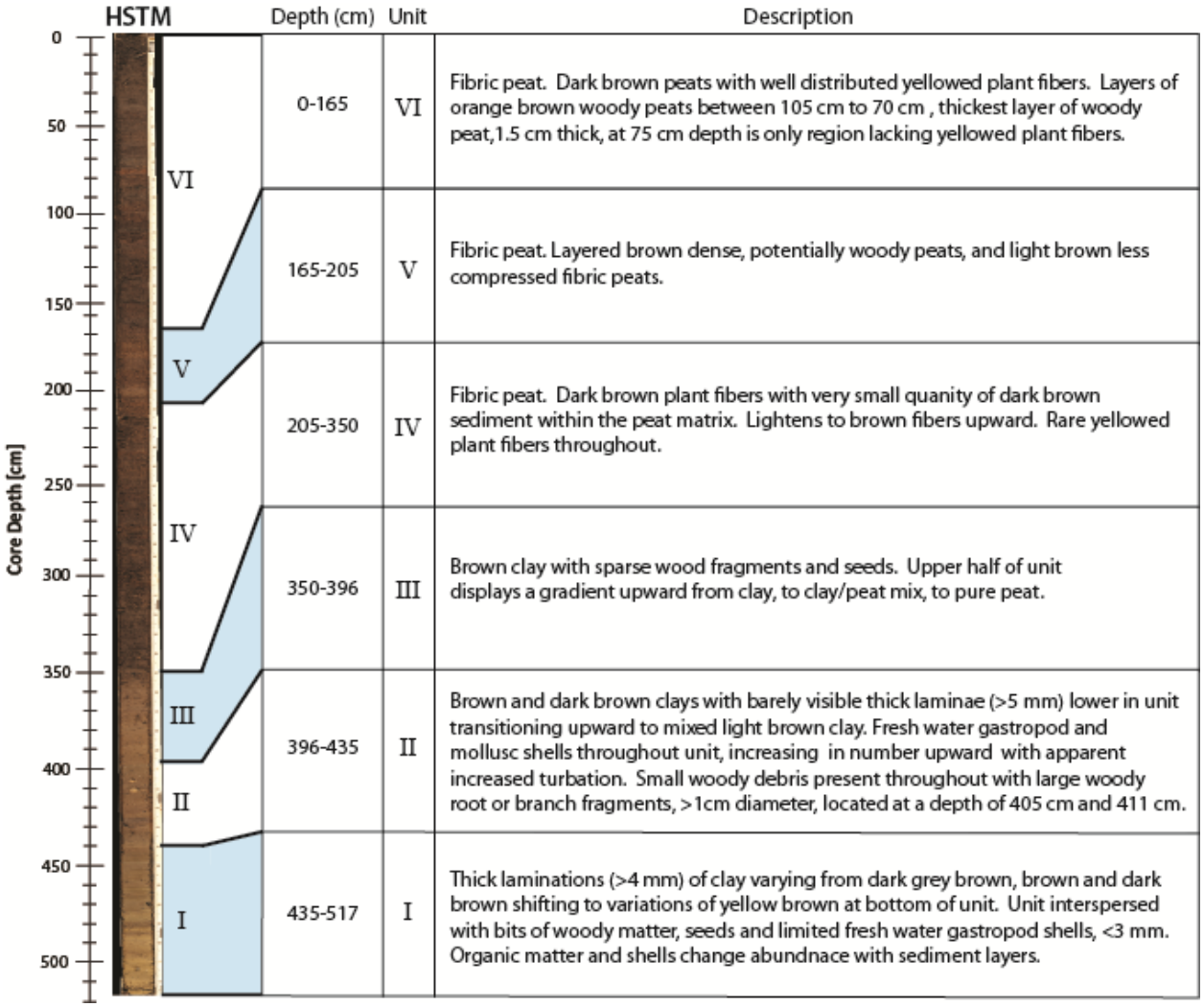

Depth (cm)	Unit	Description
0-165	VI	Fibric peat. Dark brown peats with well distributed yellowed plant fibers. Layers of orange brown woody peats between 105 cm to 70 cm , thickest layer of woody peat,1.5 cm thick, at 75 cm depth is only region lacking yellowed plant fibers.
165-205	V	Fibric peat. Layered brown dense, potentially woody peats, and light brown less compressed fibric peats.
205-350	IV	Fibric peat. Dark brown plant fibers with very small quanity of dark brown sediment within the peat matrix. Lightens to brown fibers upward. Rare yellowed plant fibers throughout.
350-396	III	Brown clay with sparse wood fragments and seeds. Upper half of unit displays a gradient upward from clay, to clay/peat mix, to pure peat.
396-435	II	Brown and dark brown clays with barely visible thick laminae (>5 mm) lower in unit transitioning upward to mixed light brown clay. Fresh water gastropod and mollusc shells throughout unit, increasing in number upward with apparent increased turbation. Small woody debris present throughout with large woody root or branch fragments, >1cm diameter, located at a depth of 405 cm and 411 cm.
435-517	I	Thick laminations (>4 mm) of clay varying from dark grey brown, brown and dark brown shifting to variations of yellow brown at bottom of unit. Unit interspersed with bits of woody matter, seeds and limited fresh water gastropod shells, <3 mm. Organic matter and shells change abundnace with sediment layers.

Housatonic and Ten Mile River Core Description. On left is brightened compiled core photo taken after a 1 day drying period. Depth measured in compressed core depth.

Appendix 10 MHR Grain Size Analysis

Sample	Sample Depth in Core (cm)	Mass Finer 63 µm (g)	Mass Coarser 63 µm (g)	% < 63 µm	% organic	D10 [µm]	D50 [µm]	D90 [µm]	D50 Full Suspension velocity (m/s)
MHR-10	10	4.06	1.38	74.6%	40.2%	123	298	777	2.275
MHR-20	20	3.29	1.24	72.6%	40.4%	144	356	829	2.859
MHR-35	35	15.37	5.56	73.4%	20.58%		179	452	1.114
MHR-44	44	4.14	52.55	7.3%	1.9%		546	9270	4.713
MHR-49	49	7.14	10.8	39.8%	16.9%		393	859	3.230
MHR-53	53	4.02	30.45	11.7%	2.3%		436	2428	3.656
MHR-57	57	5.22	7.85	39.9%	8.0%		251	838	1.806
MHR-61	61	3.86	21.09	15.5%	2.2%		690	14572	5.995
MHR-67	67	10.65	8.08	56.9%	5.1%		157	481	0.915
MHR-71	71	7.83	3.38	69.8%	6.7%		146	398	0.818
MHR-85	85	4.87	5.56	46.7%	6.2%		196	524	1.273
MHR-92	92	4.06	0.88	82.2%	15.6%		129	263	0.674
MHR-100	100	23.65	13.45	63.7%	2.6%		152	371	0.870
MHR-114	114	12.41	5.98	67.5%	5.1%		196	375	1.273
MHR-131	131	9.06	3.22	73.8%	6.8%		133	442	0.707
MHR-140	140	10.73	2.27	82.5%	9.8%		129	314	0.674
MHR-152	152	11.3	0.8	93.4%	8.3%		121	338	0.608
MHR-164	164	11.33	3.9	74.4%	9.0%	99	186	394	1.179
MHR-170	170	8.17	4.52	64.4%	7.4%		156	521	0.906
MHR-176	176	11.97	18.18	39.7%	5.3%		171	181	1.041
MHR-177	179	11.81	12.86	47.9%	5.1%		207	970	1.378
MHR-185	185	11.55	14.9	43.7%	5.3%	110	232	5259	1.620
MHR-199	199	8.65	9.37	48.0%	6.6%	104	207	660	1.378
MHR-209	209	13.96	22.57	38.2%	5.5%		115	214	0.560
MHR-218	218	8.09	1.31	86.1%	5.8%		115	238	0.560
MHR-237	237	11.23	1.2	90.3%	10.0%		123	363	0.624
MHR-240	240	13.19	3.27	80.1%	7.7%	109	224	605	1.542
MHR-254	254	8.45	1.71	83.2%	7.9%		130	306	0.682
MHR-265	265	7.95	47.3	14.4%	0.3%		446	1865	3.755
MHR-268	268	3.6	0.33	91.6%	16.6%		211	717	1.416
MHR-274.5	274.5	24.07	4.36	84.7%	7.4%		250	516	1.797
MHR-279	279	14.74	1.32	91.8%	8.7%	137	398	1150	3.280
MHR-283	283	18.63	0.73	96.2%	5.8%		204	646	1.349
MHR-288	288	15.44	3.26	82.6%	6.4%	115	225	472	1.551
MHR-295	295	8.94	15.46	36.6%	1.5%		144	244	0.801
MHR-301	301	37.09	3.38	91.6%	4.9%		119	284	0.592
MHR-305	305	2	1.73	53.6%	2.3%		225	5759	1.551
MHR-309	309	10.1	3.93	72.0%	13.3%	88	175	507	1.077
MHR-312	312	27.01	9.85	73.3%	11.5%	84	160	561	0.941
MHR-314	314	8.21	6.43	56.1%	7.6%	85	149	361	0.844

Appendix 11 WRRS Grain Size Analysis

Sample	Sample Depth in Core (cm)	Mass Finer 63 µm (g)	Mass Coarser 63 µm (g)	% < 63 µm	% organic	Sample enough for Grain Size	D10 [µm]	D50 [µm]	D90 [µm]	D50 Full Suspension velocity (m/s)
WRRS-9	9	0.52	0.02	96.3%	87.5%	N				
WRRS-13	13	0.53	0.13	100.0%	88.7%	Y	121	295	660	2.25
WRRS-20	20	0.34	0.08	81.0%	90.1%	Y	95	212	768	1.43
WRRS-25	25	9.16	0.1	98.9%	94.3%	Y	112	255	553	1.85
WRRS-31	31	0.23	0.01	95.8%	88.5%	N				
WRRS-36	36	9.24	0.05	99.5%	95.5%	Y	176	360	702	2.90
WRRS-49	49	0.22	0.09	71.0%	92.0%	Y	131	309	594	2.39
WRRS-54	54	0.79	0.21	79.0%	91.7%	Y	136	237	619	1.67
WRRS-60	60	8.51	0.26	97.0%	83.1%	Y	161	357	683	2.87
WRRS-63	63	1.35	0.2	87.1%	83.8%	Y	119	353	1729	2.83
WRRS-71	71	0.64	0.19	77.1%	85.1%	Y	132	310	902	2.40
WRRS-74	74	0.46	0.01	97.9%	90.5%	Y	106	237	440	1.67
WRRS-82	82	0.78	0.04	95.1%	85.1%	Y	175	352	973	2.82
WRRS-88	88	0.63	0.03	95.5%	85.1%	Y	125	324	694	2.54
WRRS-93	93	1	0.05	95.2%	80.5%	Y	124	275	478	2.05
WRRS-96	96	9.25	0.08	99.1%	90.7%	Y	150	345	634	2.75
WRRS-100	100	0.3	0	100.0%	94.1%	N				
WRRS-104	104	0.17	0	100.0%	94.1%	N				
WRRS-109	109	0.24	0	100.0%	91.4%	N				
WRRS-116	116	0.48	0.06	88.9%	84.9%	N				
WRRS-125	125	1.32	0.17	88.6%	78.0%	Y	80	122	367	0.62
WRRS-133	133	0.82	0	100.0%	78.6%	N				
WRRS-141	141	4.39	0.78	84.9%	36.4%	Y	86	143	412	0.79
WRRS-151	151	8.44	3.07	73.3%	26.3%	Y	101	215	557	1.45
WRRS-157	157	5.42	2.39	69.4%	24.7%	Y	93	194	705	1.25
WRRS-165	165	8.16	3.05	72.8%	27.5%	Y	99	224	590	1.54
WRRS-170	170	3.81	2.2	63.4%	23.6%	Y	112	259	867	1.89
WRRS-178	178	4.7	2.95	61.4%	27.0%	Y	100	222	664	1.52
WRRS-181	181	7.88	5.34	59.6%	21.7%	Y	117	298	1288	2.28
WRRS-188	188	5.89	3.95	59.9%	25.0%	Y	98	210	1163	1.41
WRRS-195	195	5.19	3.11	62.5%	22.2%	Y	104	229	716	1.59
WRRS-200	200	6.56	10.74	37.9%	16.7%	Y	115	296	3671	2.26

Appendix 12 SBQB Grain Size Analysis

Sample	Sample Depth in Core (cm)	Mass Finer 63 µm (g)	Mass Coarser 63 µm (g)	% < 63 µm	% organic	D10 [µm]	D50 [µm]	D90 [µm]	D50 Full Suspension velocity (m/s)
SBQB-10	10	2.42	3.56	40.47%	38.4%	110	194	368	1.25
SBQB-16	16	1.93	8.77	18.04%	10.5%	105	193	400	1.24
SBQB-20	20	0.48	12.26	3.77%	8.5%	142	441	3241	3.71
SBQB-29	29	0.83	0.38	68.60%	88.1%	93	180	373	3.40
SBQB-40	40	0.67	0.58	53.60%	75.7%	109	221	513	1.51
SBQB-50	50	4.39	2.88	60.39%	8.9%	94	168	341	1.01
SBQB-58	58	2.92	9.32	23.86%	13.5%	97	168	358	1.01
SBQB-69	69	4.03	6.43	38.53%	19.0%	101	176	365	1.09
SBQB-75	75	1.96	31.77	5.81%	1.5%	148	555	2946	4.80
SBQB-80	80	3.45	10.39	24.93%	7.9%	95	158	341	0.92
SBQB-83	83	2.84	13.84	17.03%	5.5%	99	175	423	1.08
SBQB-87	87	2.7	12.43	17.85%	5.1%	96	171	568	1.04
SBQB-91	91	1.25	12.26	9.25%	1.7%	96	170	978	1.03
SBQB-96	96	2.38	24.74	8.78%	1.7%	97	162	456	0.96
SBQB-102	102	4.53	4.58	49.73%	19.7%	88	139	247	0.76
SBQB-115	115	1.69	2.32	42.14%	28.9%	99	173	378	1.06
SBQB-119	119	3.05	7.82	28.06%	9.8%	92	149	350	0.84
SBQB-129	129	2.85	19.47	12.77%	2.5%	97	171	534	1.04
SBQB-137	137	3.68	6.13	37.51%	5.0%	87	135	279	0.72
SBQB-143	143	4.96	4.61	51.83%	13.4%	89	148	284	0.84
SBQB-150	150	4.83	6.31	43.36%	6.8%	92	156	351	0.91
SBQB-156	156	4.76	6.59	41.94%	7.6%	101	191	509	1.23
SBQB-160	160	3.38	8.2	29.19%	5.0%	98	183	503	1.15
SBQB-174	174	3.69	8.71	29.76%	5.3%	104	197	544	1.28
SBQB-183	183	3.16	6.98	31.16%	7.2%	97	181	540	1.13
SBQB-197	197	4.1	9.64	29.84%	6.9%	99	202	678	1.33
SBQB-209	209	3.28	7.37	30.80%	7.6%	102	203	566	1.34
SBQB-222	222	3.3	11.75	21.93%	4.8%	104	217	809	1.47
SBQB-227	227	3.35	12.93	20.58%	3.8%	100	201	586	1.32
SBQB-233	233	3.64	15.71	18.81%	3.8%	107	216	746	1.46
SBQB-244	244	6.31	10.69	37.12%	7.0%	107	209	478	1.40

Appendix 13 Projected Flood Widths

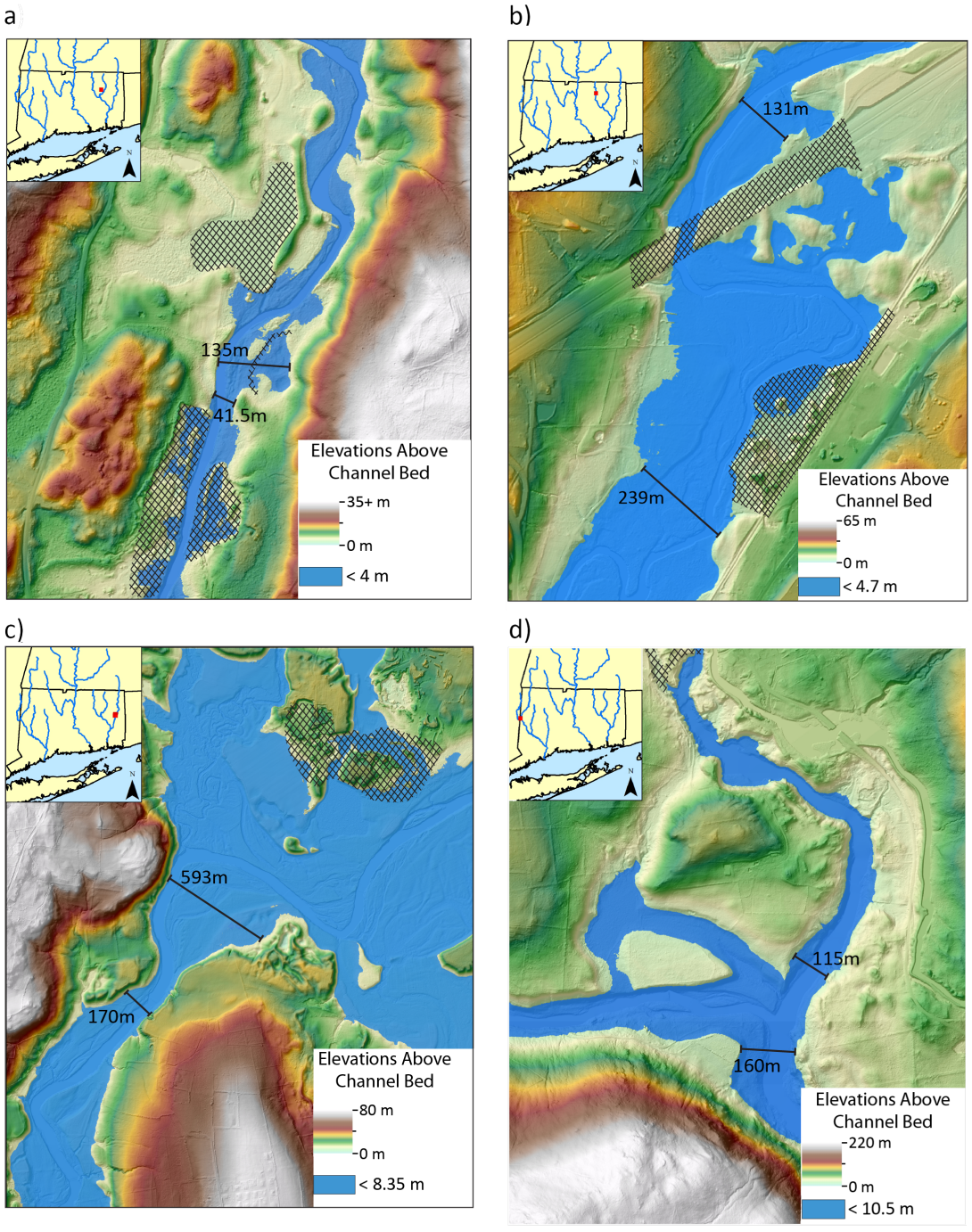

Flood widths measured using flood depths projected onto altered DEM so elevations are in respect to channel bed. a) is MHR b) is WRRS, c) is SBQB and d) is HSTM.

Appendix 14 Quinebaug Terrace Flood Extent

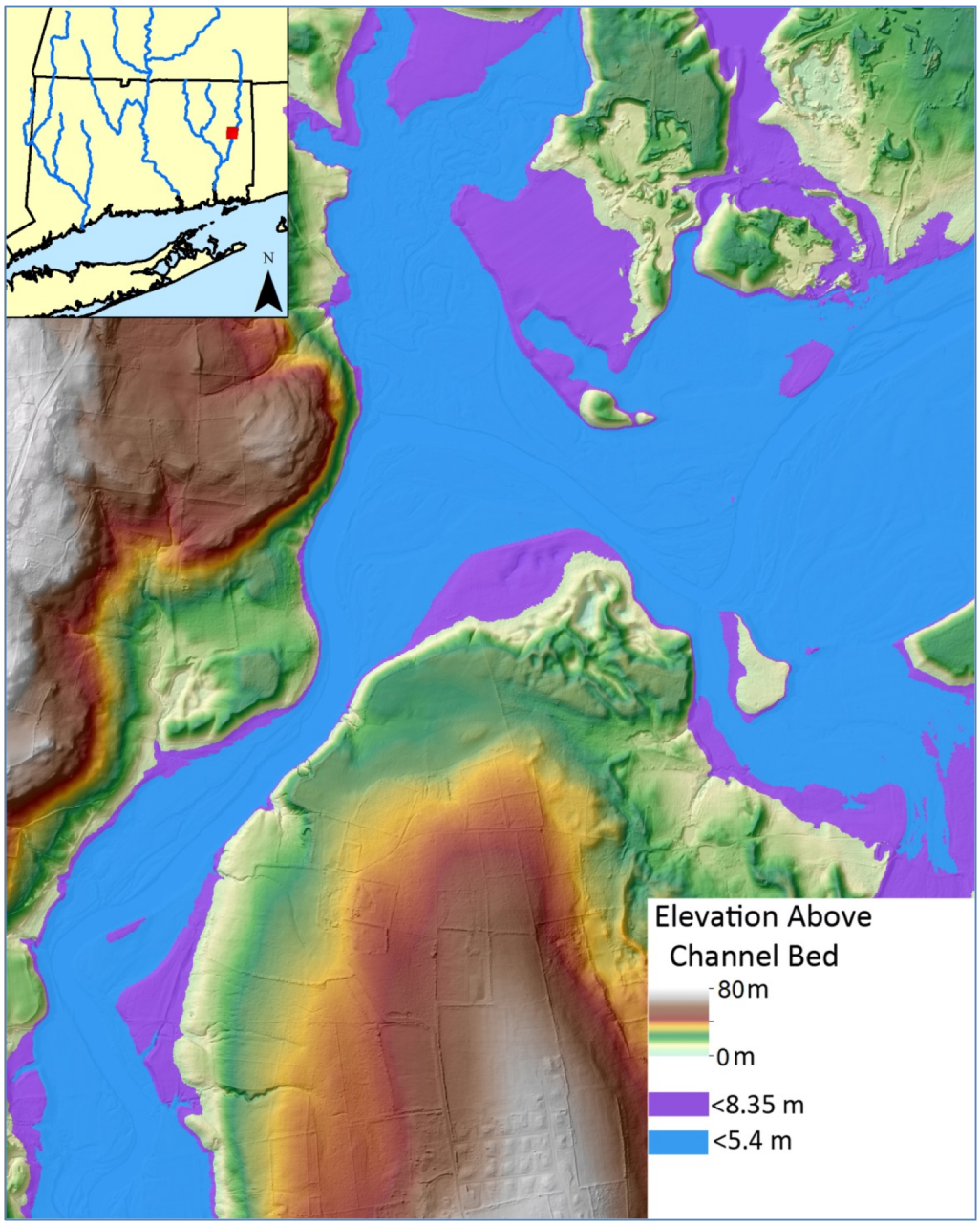

Extent of inundation from floods which cover the upper terrace at SBQB (purple) and which covers the lower terrace (blue)

Appendix 15 River Discharge Rating Curves

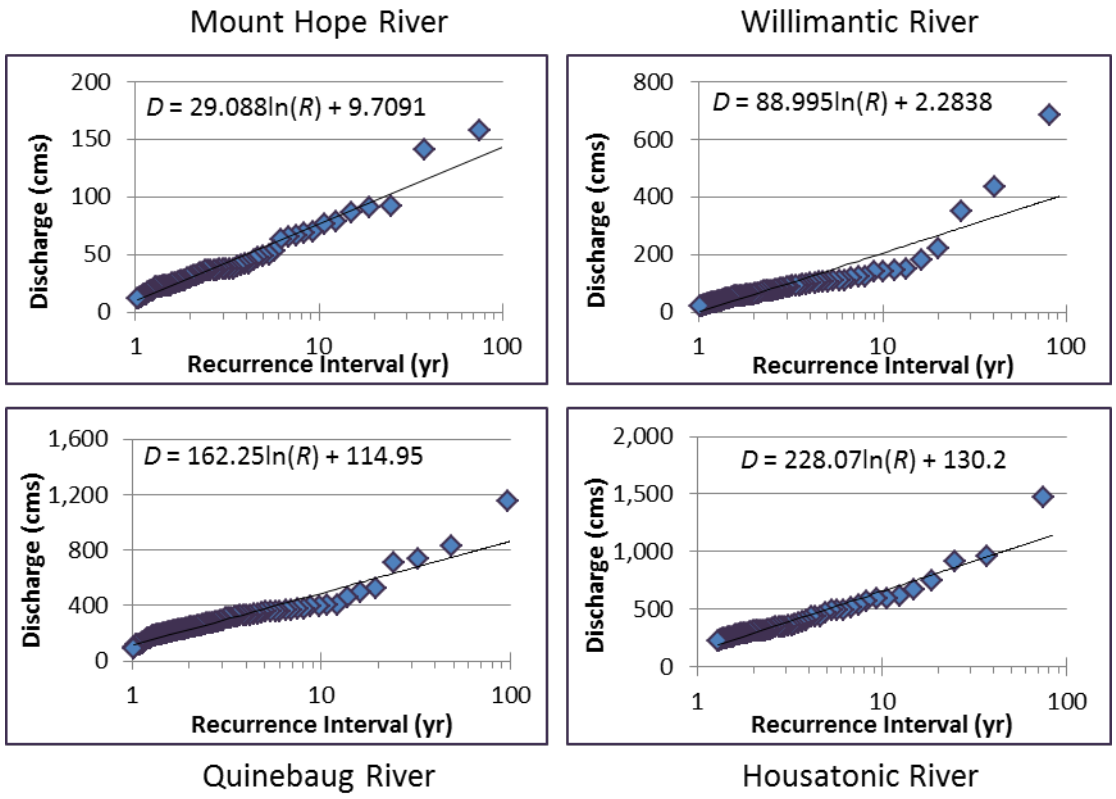

Annual Peak Discharge Recurrence Intervals from Modern Gage Station. The trend line is governed by the equation for discharge *D* and recurrence interval *R.* Mount Hope River data (upper left) from USGS station 01121000 near Warrenville, CT, 2.5 miles upstream of field site. Willimantic River data (upper right) from USGS station 01119500 near Coventry, CT, 9.81 miles downstream of field site. Quinebaug River data (lower left) from USGS station 01127000 at Jewett City, CT, 8.66 miles downstream of field site. Housatonic River data (lower right) from USGS station 01200500 at Gaylordsville, CT, 21.8 miles upstream of field site

Appendix 15 Southern New England Watersheds

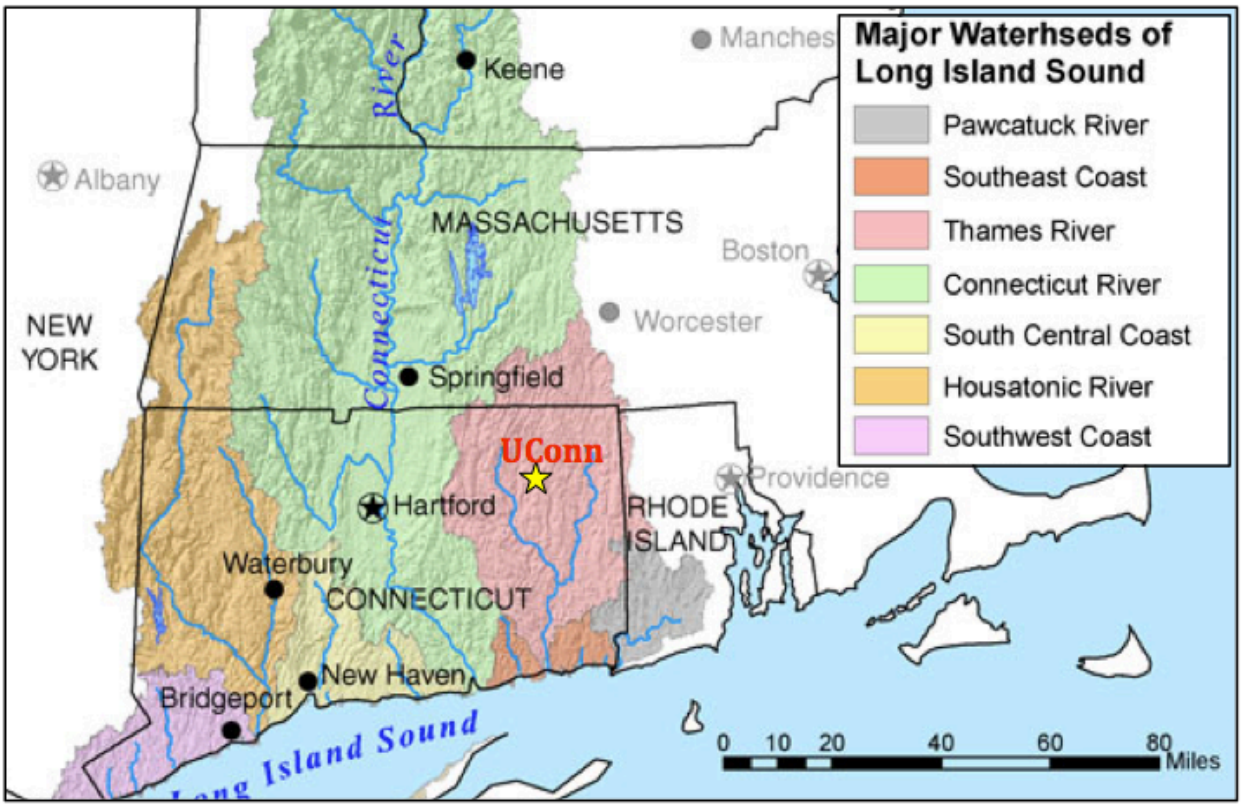

Mod Ouimet, 2015